ARMY RESEARCH LABORATORY

Construction and Testing of the ARL 1.68-m Diameter Shock Tube Exit Jet Spreader for Non-Ideal Blast Simulation

John A. Condon
Richard E. Lottero
Richard B. Loucks

ARL-TR-1336 JUNE 1997

The findings in this report are not to be construed as an official Department of the Army position unless so designated by other authorized documents.

Citation of manufacturer's or trade names does not constitute an official endorsement or approval of the use thereof.

Destroy this report when it is no longer needed. Do not return it to the originator.

Army Research Laboratory
Aberdeen Proving Ground, MD 21005-5425

ARL-TR-1336 June 1997

Construction and Testing of the ARL 1.68-m Diameter Shock Tube Exit Jet Spreader for Non-Ideal Blast Simulation

John A. Condon
Richard E. Lottero
Richard B. Loucks
Weapons & Materials Research Directorate

Abstract

The U.S. Army Research Laboratory (ARL) has demonstrated the feasibility of using the modified exit jet of a simple shock tube to simulate high dynamic pressure air blast flows such as those that occur in non-ideal nuclear blast events. These flows can be used to generate simulated non-ideal blast loads on Army equipment with the intent of evaluating and improving its survivability. This work has included the use of small, intermediate, and large scale shock tubes to which exit jet spreader devices were incorporated. These spreaders were mounted at the ends of the shock tubes but were not directly connected to them. Their purpose was to spread the exit jets and their associated dynamic pressure impulses more uniformly over a greater area, thus providing a more accurate simulation capability for testing larger targets.

This report documents some of the latest efforts by ARL in evaluating the use of modified shock tube exit jets for simulating non-ideal blast flow. Previous studies at ARL included the mapping of unspread exit jets at three different shock tube scaled sizes and the evaluation of exit jet spreaders at the two smaller shock tube sizes to evaluate the effectiveness of the various spreaders and determine the degree of uniformity of the spreading. In the latest effort, a full scale exit jet spreader has been constructed for use with the ARL 1.68-m diameter shock tube, the largest of the three shock tubes. Displacement experiments with World War II Army jeeps have been conducted to compare vehicle response to the dynamic pressure impulse loading generated by the spread jet of the shock tube with that from past actual and simulated nuclear tests in which jeep displacement data were obtained.

ACKNOWLEDGMENTS

The authors would like to thank the following ARL employees: Mr. Peter Muller, Mr. William Sunderland, Mr. Richard Thane, Mr. L. Gene Ferguson, Mr. Christopher Mermagen, and Mr. Timothy Cline; and Dynamic Science, Incorporated, employee, Mr. Paul Neumann, for their contributions in various ways throughout the construction and testing phases of this project. Their individual talents and support were very much appreciated, as was the technical review of this report by Mr. Stephen Schraml of ARL.

The authors would also like to thank Mr. Noel Ethridge and Mr. John Keefer of Applied Research Associates for their advice and support during the testing. Their services as retired scientists and colleagues from the former U.S. Army Ballistic Research Laboratory in the planning and layout of the cubes to indicate dynamic pressure impulse and analysis of the cube displacements were donated at no cost to ARL.

INTENTIONALLY LEFT BLANK

TABLE OF CONTENTS

INTENTIONALLY LEFT BLANK

LIST OF FIGURES

INTENTIONALLY LEFT BLANK

LIST OF TABLES

INTENTIONALLY LEFT BLANK

1. INTRODUCTION

When a shock wave exits a shock tube and expands into the surrounding atmosphere, a strong, transient exit jet is formed behind it. If the flow behind the shock while it is still inside the shock tube is locally subsonic, then an expansion wave originates at the exit plane and moves upstream against the flow into the shock tube. The shock tube flow through which this expansion wave travels is thereby accelerated, with a corresponding decrease in static overpressure and increase in dynamic pressure. For studies involving shock wave diffraction and drag loading on targets placed inside of the shock tube, this effect is usually undesirable. The arrival of such an expansion wave at the test section inside the shock tube often means that the valid, desired simulation time has ended. For studies of blast loading on relatively large targets placed outside the exit of a shock tube, it has often been necessary to take precautions to keep the target off to the side and away from the relatively strong exit jet centered on the axis of the shock tube. This report documents recent studies by the former Blast/Thermal Effects Branch of the U.S. Army Research Laboratory (ARL) that began under the previously named Blast Dynamics Branch of the U.S. Army Ballistic Research Laboratory (BRL). BRL was integrated into ARL in October 1992, and the Blast/Thermal Effects Branch was disbanded in October 1996. Part of the mission of that branch had been to develop technology to simulate both "ideal" and "non-ideal" air blast from nuclear bursts above ground at ideal blast shock overpressure levels of tactical interest, defined as overpressures of 241.3 kPa (35.0 psi) and below. This report documents the investigation of the use of shock tube exit jets as one of the possible ways to simulate non-ideal blast waves, at least in the tactical overpressure range. First, brief descriptions of (1) the principal features of ideal and non-ideal blast, (2) previous work involving shock tube exits jets, and (3) a view of how this exit jet study fits into the overall approach to simulating nuclear air blast at tactical overpressure levels are given before the results of this study are presented.

1.1. Ideal Versus Non-Ideal Air Blast

Air blast waves of military interest are typically produced by either the detonation of conventional high explosives or by the surface or airburst of a nuclear device. Neglecting dust and debris, a conventional high explosive typically produces an ideal blast wave in its far-field region (i.e., away from the fireball produced by the detonation products). The current nuclear survivability requirements for Army tactical vehicles and structures are based on ideal blast loading events.

Ideal blast from a nuclear device is defined as that which does not include any thermal, dust, or debris layers that modify or augment the dynamics or the structure of the air blast wave as it moves across the ground plane. In typical low altitude nuclear burst events above land, a heated layer is formed just above the ground by the interaction of the thermal radiation pulse with the ground surface. The intensity and extent of this thermal layer are highly dependent upon factors such as soil type, vegetation, moisture content, local topography, and the ability of the surface to re-radiate energy back into the atmosphere immediately above the ground surface. This heated layer is then struck by the blast wave

which follows the thermal pulse, and a complex interaction then occurs. The portion of the shock front that strikes the heated layer is accelerated and weakened. Consequently, it runs ahead of the remainder of the shock front, forming a precursor region. At the point where this weakened precursor shock connects back to the undisturbed incident shock, a shear layer is formed at an appropriate angle to equilibrate the flows behind the two unequal shocks. This interaction generates at least a singly bifurcated, high dynamic pressure flow along the ground surface, scouring the surface, and lofting and accelerating soil and debris. This is referred to as non-ideal blast. The reader is referred to Glasstone and Dolan[1] for a more complete description of nuclear weapon effects. A review by Bryant and Allen[2] of the dynamic pressure impulse delivered by ideal versus non-ideal blast from above-ground nuclear tests showed that non-ideal blast delivered as much as five or more times the impulse for the same blast wave over an ideal surface for blast overpressures of tactical interest. Recently, ARL funded contract studies to analyze the 36.6-kT atmospheric nuclear event PRISCILLA. An excellent unclassified summary of the history of nuclear weapons and events, including the PRISCILLA event, has been published by Shelton.[3] Data from the actual PRISCILLA event were compared with SHARC[4] hydrocode computations simulating a near-ideal versus desert surface,[5] a near-ideal versus grassland surface,[6] and then a detailed summary report[7] that contained a complete analysis of the actual PRISCILLA event data and comparison with the three SHARC computations. The analysis corroborated the earlier analysis[2] that indicated the large increase in dynamic pressure impulse in non-ideal blast over that in ideal blast. Both analyses also showed that blast damage radii for drag phase loading for a non-ideal nuclear blast event can extend well beyond the radii predicted for an ideal blast event. This could result in an overly optimistic estimate of the survivability of a tactical force operating in terrain that is capable of producing non-ideal blast. An example is a tactical force operating in a desert area that is attacked by an above-ground nuclear burst. This unit should expect to experience such a non-ideal blast event.

Nuclear blast waves are often simulated in a somewhat simplified way through the use of shock tubes, which can be driven by either compressed gas or other energy sources. The interaction of a classic, or ideal, blast wave with a target vehicle or structure can be characterized as occurring in two distinct phases: an initial diffraction phase and a subsequent drag phase. The damage mechanisms from actual nuclear airburst events include thermal loading; blast diffraction loading; drag phase loading; neutron, gamma, and residual radiation effects; electromagnetic pulse; and other effects. Only the blast flow and its simulation are of direct interest in this discussion.

Diffraction loading occurs during the interaction of a shock front with either a target vehicle or moderately sized structure. This loading phase typically lasts for, at the very most, a few tens of milliseconds while the shock passes over the target and rarefaction waves traverse the loaded faces to relieve the reflected shock pressures. Relatively little of the total integrated impulse from a nuclear blast wave is delivered during this time, at least in blast waves from typical threat weapons of tactical interest for armored vehicles. Total integrated impulse is defined as the double integral over the time and space of the pressure loading on the target surface. The threat from the diffraction phase loading to a conventional armored vehicle is limited to damage to components such as some types of antennas and relatively light sheet metal components. Light targets such as trucks and communications

shelters could be directly threatened by the shock diffraction process. Whether the shock diffraction loading could cause meaningful deflection or damage to composite sheets that were part of a composite armored vehicle structure would have to be examined on a case-by-case basis. While it is unlikely that the shock diffraction loading is a great threat to most armored vehicles themselves, it could limit their utility if communications were lost. Also, if light sheet metal or composite panels were used as skirts around the road wheels and tracks, consideration must be given to the possibility of their being blown into rotating or translating components that could be jammed by debris. A non-ideal blast event typically has reduced diffraction phase loading, with the action of the thermal layer causing a reduction in the incident shock overpressure as part of the repartitioning of energy into an increase in dynamic pressure and the lofting and acceleration of dust and debris.

Drag phase loading occurs immediately after the end of the diffraction phase. A classical free air blast wave has an exponentially decaying accelerated flow region behind the incident shock front. This continues for a period referred to as the "positive phase duration," at the end of which the static pressure declines through that for ambient atmospheric pressure and becomes sub-atmospheric for a time referred to as the "negative phase duration." A tactical nuclear blast wave can have a positive phase duration lasting from a few hundred milliseconds to a few seconds. It is during this time that the majority of the total integrated dynamic pressure impulse, hereinafter referred to as "dynamic pressure impulse" for simplicity, is delivered to a target. The primary threat to an armored vehicle from the drag phase is translation and overturning of the vehicle, with a possibility of loss of both crew and vehicle. The introduction of lighter weight composite vehicles will make it even more necessary to evaluate drag phase loading because such vehicles would have a greater tendency to overturn than a heavier armored vehicle with the same cross section and drag coefficient subjected to the same blast event. Taking steps to reduce the drag coefficients of tactical vehicles is unlikely to have ever been seriously considered in the past. Now, it is highly appropriate to consider it for vehicles that have nuclear survivability criteria. A classic example of the reduction of a forward travel drag coefficient to 0.42 from 0.76 for a van, with only minor changes in rounding of corners on the vehicle, is given by Schlichting.[8] The primary overturning threat to a vehicle is from a blast striking it from the side, but the drag coefficient effects are the same as for the illustrated example. The drag loading at any instant is computed by multiplying the drag coefficient times the dynamic pressure times the presented area.

After accounting for the direct output of nuclear radiation energy, the remaining energy partition from a non-specific nuclear device is approximately equal in thermal and blast output. For reasonable tactical threat devices and ranges, the thermal pulse arrives at the target any time between several hundred milliseconds to a few seconds before the blast wave, depending on the weapon design and yield. The immediate damage to structures from the thermal loading can include incendiary effects, distortion because of thermal stresses, destruction of optical devices, delamination, and general depreciation of material strength. The delayed effects, which interact synergistically with the following blast pulse, can include weakening of metals, thermal stresses, melting of glues on layered materials, softening of the matrix in a composite material, and debonding of composite layers. This can make a structure much more susceptible to damage to the following blast pulse than it might have

otherwise been. The synergistic effects of a properly timed thermal/blast loading have been shown to be considerably greater that the individual effects of only blast and only thermal loading.[9]

This combined thermal/blast event is referred to as non-ideal blast. It also includes a lofting and scouring of debris, soil, and loose material that contributes greatly to the loading on any vehicle or structure. A desert terrain would be ideal for generating a non-ideal blast wave, as would grassland or cropland.

1.2. Previous Work With Shock Tube Exit Jets

Researchers have found that the high dynamic pressure flows in shock tube exit jets can be useful for simulating blast flows such as those found in non-ideal nuclear blast events. One such use of a modified exit jet was suggested by Newell.[10] This involves a straight shock tube with a coaxial driver, two-diaphragm system, wherein the downstream section of the driver is at one half of the pressure of the upstream (i.e., farthest from the exit) section of the driver. The diaphragm of the downstream driver section is burst on command, and then the upstream diaphragm is burst naturally by the one-sided pressure relief caused by the arrival of the expansion wave on its downstream side. This sequential opening of the two diaphragms sends a relatively weak shock and flow downstream, followed by a second flow overriding it, with the composite flow accelerated upon exiting the shock tube. With proper timing, this concept showed promise for generating an exit jet with a two-stage dynamic pressure history similar to that seen in a non-ideal blast flow.

Kingery and Gion[11] performed a series of experiments with a 2.54-cm (1.0-inch) diameter shock tube to document the dynamic and static pressure impulse properties of the exit jet for a variety of driver pressures. Impulse is computed by integrating the appropriate pressure history, either static or dynamic, over time. The exit jets were shown to be highly collimated for several shock tube exit diameters downstream from the exit plane. Typically, the dynamic pressure impulse along the centerline was much larger than the impulse for static overpressure (therein referred to as "side-on pressure"), with a very sharp decrease of dynamic pressure impulse for radial distances (i.e., distances normal to the axis of symmetry of the shock tube), greater than the exit radius of the shock tube. One example given[11] was "At a distance where 10.3-kPa (1.5-psi) side-on pressure was measured, a 49.6-kPa (7.2-psi) stagnation pressure was measured. At the same distance, a side-on impulse was 12.6 kPa-ms (1.83 psi-ms), while the stagnation impulse was 134 kPa-ms (20.2 psi-ms) – a dramatic difference." In that report, the dynamic pressure was taken to be a simple difference of the stagnation pressure, P_0, and the absolute static pressure p_s, or

$$q = P_0 - p_s, \tag{1}$$

which is often done in the literature, especially that reporting actual or simulated nuclear event blast measurements, even for flows which can have significant compressibility effects. This term, q, will hereinafter be referred to as the "differential pressure." The impulse computed by integrating q over time will hereinafter be referred to as the "differential pressure impulse" and given the symbol I_q. The more rigorous, classical definition of dynamic pressure

is

$$Q = \frac{\rho v^2}{2}, \tag{2}$$

in which ρ is the static density and v is the particle velocity. Dynamic pressure impulse is obtained by integrating Q over time, and is represented by the symbol I_Q. The historical data for jeep displacement, discussed later in this report, used the differential pressure impulse, I_q, as a basis for relating displacement to dynamic pressure impulse, with some corrections for compressibility effects. Therefore, to have a direct comparison to the historical work, the current study also uses the average, measured differential pressure impulse as one of the two indicators of dynamic pressure impulse along with cube displacement data. This is discussed in detail later in this report. For low speed flows with only minor compressibility effects, the differences between q and Q are small and are often within the error bar of the experimental measurements.

Kingery and Gion[12] also performed a follow-on study of the effects of interior static overpressure wave shape on exit jet dynamic pressure impulse. In addition to using a long driver to produce a non-decaying "flat-top" shock inside the driven section of a 2.54-cm diameter shock tube, they also used a relatively short driver to produce a decaying blast wave inside the shock tube. Both showed dynamic pressure increases in the exit jet, with the decaying wave having less of an increase, as might be expected. In a later study, Gion and Kingery[13] placed a model barricade in front of the exit jet from a 2.54-cm diameter shock tube. Their primary purpose was to measure the disruption of the exit jet from a simulated explosion event in a munitions magazine. Enhanced dynamic pressures were also observed in that study in reference tests where the barricade was removed. Previously, Kingery had recognized that these enhanced dynamic pressure flows in shock tube exits jets resembled those observed in previous above-ground nuclear testing. He proposed[14] that consideration be given to extending the operational capabilities of the (then) BRL 1.68-m diameter shock tube to develop technology to simulate non-ideal nuclear blast flows with modified shock tube exit jets. A 1992 firing[15] of the unspread exit jet from the ARL 1.68-m shock tube on an M-113 armored personnel carrier (APC) demonstrated this well. The APC had a mass of about 10,430 kg (23,000 lbm, where lbm denotes pounds mass, avoirdupois). It was placed on the ground plane with its left face oriented normal to and centered in its presented area on the axis of symmetry of the shock tube, 15.2 m (50 ft) from the exit plane of the shock tube. At that time, the ground plane was approximately 0.84 m (2.75 ft) below the bottom of the shock tube exit. The driver gauge pressure was 572.3 kPa (83.0 psi). The APC was thrown 39.8 m (130.5 ft) from its original position, with the majority of the travel airborne.

A contract sponsored by the Blast Dynamics Branch, Terminal Ballistics Division, of BRL was awarded in 1989 to Applied Research Associates, Inc., to study the feasibility of using the exit jet of the 1.68-m shock tube for simulating the high dynamic pressure and relatively low static overpressure flow observed in non-ideal nuclear blast. This study, documented by Ethridge,[16] involved the construction of a scaled model of the 1.68-m shock tube, the mapping of its unmodified exit jet, the design of candidate exit jet spreaders, and the mapping of those modified exit jets. The study showed that it was technically feasible to produce a uniformly spread exit jet from a small scale shock tube. Subsequently, a scaled model of a candidate jet spreader designed to fit on the ARL 10.16-cm diameter shock tube

was delivered to ARL for evaluation.

The ARL 10.16-cm diameter shock tube was constructed specifically as a 1:16.5 scale model of the ARL 1.68-m diameter shock tube as part of a mission program to develop non-ideal blast simulation technology using shock tube exit jets. At the time it was built, there was still some uncertainty as to whether or not the unmodified exit jet flows would scale with one another in an orderly fashion, and, more specifically, whether a small scale jet spreader design would also work at the large scale of the 1.68-m shock tube. Studies were performed to map the unmodified exit jets of the 1.68-m and 10.16-cm shock tubes. The jets were found to scale directly in both physical dimensions, dynamic pressure impulse, and time. The candidate jet spreader designed and constructed by Ethridge based on an extension of his earlier work[16] was tested on the 10.16-cm shock tube. It was determined that it was capable of producing a uniformly spread exit jet. However, its design involved a large bundle of adjustable tubes, grouped in subassemblies of tubes, that appeared to be too complex and costly to construct at the scale of the 1.68-m shock tube, given the time and funding constraints. A simpler gas dynamic design using a diverging rectangular box for an outer shell and a series of interior deflectors made of angle irons was suggested,[17] constructed by Mr. R. Thane of ARL, tested, and modified by ARL researchers to get the best performance. This design was ultimately selected as the most effective and practical. It was tested at an intermediate scale at the end of the ARL 0.61-m (24-inch) diameter shock tube and found to perform well and exhibit reasonably good scaling, given that this tube had a shorter driver in scaled relation to both the 10.16-cm and 1.68-m shock tubes. As a result, its jet had a relatively shorter duration and correspondingly less impulse because of its disproportionately smaller amount of driver gas. This work is documented in the report by Loucks et al.,[18] including the actual structural design of the spreader by Loucks.

During that period, a numerical study of the exit jet from the ARL 1.68-m shock tube was performed by Guidos et al.[19] This study was interesting for several reasons. First, it showed good agreement with data from gauges for the experiment that was simulated, thereby providing confidence in both the experimental measurements and the numerical simulation. Secondly, it showed that the dynamic pressure waveform is similar to those observed in actual non-ideal blast nuclear events. The static overpressure history was somewhat similar to that for non-ideal blast in that the shock front was greatly weakened by radial divergence. However, it is important to look at the dynamics of the gas flows that were present in the experiment. The driver of the 1.68-m shock tube contained high pressure air, filled slowly enough with standard air compressors so that the driver gas remained at ambient temperature. When the diaphragm was ruptured with a set of linear shaped charges, the incident shock developed quickly and traveled down the expansion section and out the exit of the shock tube. This expansion section air was heated and accelerated by the shock. Because the shock was not strong (the measured static overpressure in the expansion section was approximately 160 kPa), the expansion section gas flow behind the shock remained locally subsonic within the expansion section. Once outside the shock tube, this flow accelerated but probably did not develop any significant regions of supersonic flow, and the incident shock quickly dissipated through radial divergence. The dynamics of the driver gas are very different. Initially, it is cooled well below ambient by the passage of the rarefaction wave that is initiated by the bursting of the diaphragm, thereby decreasing its local speed of sound

below that for ambient air. There is both static pressure and particle velocity matching across the contact surface between the expansion section gas and the driver gas. Thus, the driver gas is moving at a higher local Mach number than the shocked expansion section gas. The velocity of the driver gas is further increased by the action of the rarefaction that is generated at the exit of the shock tube with the passage of the incident shock. The driver gas exited the shock tube as an under-expanded jet and accelerated further. The computation by Guidos et al.[19] indicated that the driver gas in the exit jet was supersonic, cold, and relatively dense. The dynamic pressure impulse from the exit jet of the ARL 1.68-m shock tube is dominated by driver gas flow. Thus, while the overall dynamic pressure impulse is quite similar to that for a non-ideal nuclear blast flow, there are some differences in the gas dynamics.

1.3. Relation to Other Activities and Techniques

The efforts at ARL to investigate the development of exit jets for non-ideal nuclear blast simulation were not limited to just the improvement of ARL blast simulation facilities. As stated previously, part of the mission of the Blast Dynamics Branch (later the Blast/Thermal Effects Branch) was to develop nuclear air blast simulation technology and transfer it to agencies such as the U.S. Army Test and Evaluation Command (TECOM) in cooperation with the Defense Special Weapons Agency (DSWA), previously known as the Defense Nuclear Agency (DNA). Much effort, coordinated by Mr. R. Pearson of the branch, was put into developing the gas dynamic design for the U.S. Large Blast/Thermal Simulator (LB/TS).[20] The design and logic for the gas dynamics of the LB/TS are based on the design of the large blast simulator, or *Le Simulateur de Souffle a Grand Gabarit* (SSGG)[21] at the *Centre d'Etudes de Gramat* (CEG), France. This design information was provided to the U.S. by France under a cooperative Data Exchange Annex[22] which has been most valuable to both countries in the exchange of basic phenomenology and simulation technology related to nuclear blast. The SSGG was the first large scale, multi-driver, nuclear blast wave simulation facility. Both the LB/TS and the SSGG were designed to simulate ideal nuclear blast. The studies with the exit jet were one part of an overall effort by ARL, DSWA and its contractors, and other agencies to find ways to operate the LB/TS to optionally simulate non-ideal blast without compromising its ability to simulate ideal blast. An analysis of the exit jet for the LB/TS was done by Schraml.[23] That study showed that at least an idealized LB/TS exit jet could be used to simulate a non-ideal nuclear blast flow. The LB/TS exit jet is dominated by accelerated expansion section gas that had been processed by a decaying interior blast wave, unlike the exit jet from the ARL 1.68-m shock tube which is dominated by driver gas and has a leading, long-duration flat-top shock inside the expansion section.

Other techniques that have been, or are being, evaluated to extend the operational capabilities of the LB/TS to include non-ideal blast simulation are the use of time-sequenced opening of drivers, and the use of helium layers inside the expansion section. For ideal blast simulation, the seven drivers in the CEG SSGG, and the nine drivers in the LB/TS, are opened as close to simultaneously as possible to generate the sharpest and most uniform shock front. Dr. A. Mark proposed[24] that non-ideal nuclear blast flows might be simulated

in either facility by opening subgroups of drivers in a delayed time sequence. This would generate a relatively weak leading blast wave with one or more following blast waves traveling on the previously accelerated driver and expansion section gases. With proper selection of driver groups, driver pressures, and timing, a multi-structured blast wave with a reduced shock front and an enhanced dynamic pressure history could be produced. This idea was presented[25] to representatives of the CEG staff, who, under the Data Exchange Annex,[22] agreed to evaluate that technique in the SSGG. The CEG staff was able to produce simulated non-ideal blast waves with this technique in tests on a light armored vehicle and a self-propelled gun.[26] Guided by consultative assistance, results from small-scale experiments, and computations by ARL personnel, DSWA was able to perform a similar non-ideal blast simulation[27]with staggered firing of drivers in the U.S. LB/TS. The target was an M-113 (APC), placed in the expansion section of the LB/TS. The staggered driver firing on the M-113 caused it to be translated violently down the length of the LB/TS, airborne at times, and be expelled through the open exit. An earlier shot simulating an ideal blast for a similar weapon yield and ground range had caused only minimal motion of the same APC. An evaluation[28] of a proposed technique involving the use of a helium layer on the floor of the LB/TS indicated that the resulting flow would most likely be inadequate for testing on full scale tactical vehicles.

1.4. The Current Study

In the previous ARL research,[18] it was learned that a relatively inexpensive and simple method of spreading the highly collimated exit jet from a shock tube could be developed to uniformly distribute the dynamic pressure impulse over a large target placed at some distance from the shock tube. These efforts sought to extend the capabilities of conventional shock tubes to include non-ideal blast simulation testing as well as add a new capability to facilities such as the U.S. LB/TS. This could ultimately serve as an aid in designing more survivable Army equipment. This method was successfully tested in experiments with small scale shock tubes and a concept exit jet spreader with integral spreader vanes. However, full scale test data were needed to further substantiate the theory that was successfully demonstrated in small scale. Mission funding support for the building of a full scale version of the spreader attached to the existing 1.68-m diameter shock tube at ARL was provided which allowed for the continuation of this non-ideal blast research.

The intent of this report is, first, to document the design and construction of the full scale version of the exit jet spreader, including the top, bottom, and side walls for lateral and vertical control of the direction of the flow; the integral spreader vane assembly for producing flow uniformity within the spread jet; and the independent reaction mass for the jet spreader to resist the diffraction and drag forces generated by the interaction with the exit jet. Second, the temporary pressure probe rake mounting and location are discussed, as is the new elevated ground plane that was built to bring the ground surface up to the bottom of the shock tube. Third, this report presents early test data that were obtained to evaluate and demonstrate the use of exit jets from large scale shock tubes to simulate non-ideal nuclear blast environments on Army materiel.

2. EXIT JET SPREADER DESIGN

A right side elevation view of the reinforced concrete reaction mass and jet spreader structural steel is shown in Figure 1. The reinforced concrete reaction mass contains approximately 19.9 m^3 (26 yd^3) of concrete with an estimated mass of 47,760 kg (105,300 lbm). The steel reinforcing rods (1.27-cm diameter), beams, and plates added approximately 4,540 kg (10,000 lbm), for a total mass of 52,300 kg (115,300 lbm). Figure 1 includes indications of both the ground plane location at the rear of the jet spreader (slightly upstream from the shock tube exit plane) and the elevated ground plane downstream from the exit of the jet spreader. The exit of the shock tube protrudes into the entrance of the jet spreader by 0.84 m, or one shock tube radius. The upstream end of the jet spreader that is outside the radius of the shock tube is open to allow entrainment of outside ambient air generated by the venturi effect of the exit jet. This has a dual function. First, it reduces the development of any late time sub-atmospheric pressure inside the jet spreader, thereby simplifying the structural design. Second, there is a secondary effect wherein the entrained air is mixed with the exit jet, adding mass and impulse delivery at the target that will be positioned downstream on the new, elevated ground plane.

The original ground plane had been about one shock tube radius below the bottom of the shock tube. The new ground plane vertical location is approximately flush with the bottom of the shock tube. This was accomplished by adding, compacting, and grading a large amount of stable fill dirt to form a wide plane for mounting probe rakes and placing full scale target vehicles. Earlier studies[18] showed that, in the original configuration, the jet remained nearly the same distance above ground but that this was not attributable to a gas-dynamic ground effect. This left an undesired region of low velocity flow between the ground surface and the bottom of the jet, not at all like the flow at the ground surface in an actual non-ideal blast event. Those earlier studies also showed that moving the ground plane up to the bottom of the shock tube had essentially no effect on the jet and gave the desired flow parallel to the surface, starting from the ground level. This eliminated the need for designing a jet spreader that included a redirection of flow downward toward the ground, which would then have required designing a reaction mass to resist lift as well as horizontal loading. Other problems with trying to deflect the jet toward the ground would include increased scouring of the ground surface and excessive lifting of dust and debris, and having the jet possibly reflect back upward after striking the ground. Bringing the ground plane up to the bottom of the exit of the shock tube allowed the flow to be both at, and parallel to, the surface from the start. Even so, later tests showed significant dust pickup, at least qualitatively similar to an actual non-ideal blast flow but potentially troublesome in obtaining clear video records and in pressure gauge survival and reliability.

Also shown in Figure 1 is a side view of the spreader vane assembly. It consists of two vertical, 90-degree angle irons, 15.24 cm (6.0 inches) on a side and 1.27 cm (0.5 inches) thick, oriented with each corner edge facing upstream and the bisector of the 90-degree angle parallel to the shock tube axis. The angle irons have welded-on, 9.53-mm thick, steel rib stiffeners in the interior 90-degree angle. The leading edges of these vertical angle irons are 1.5 m downstream from the exit plane of the shock tube, and each is laterally spaced

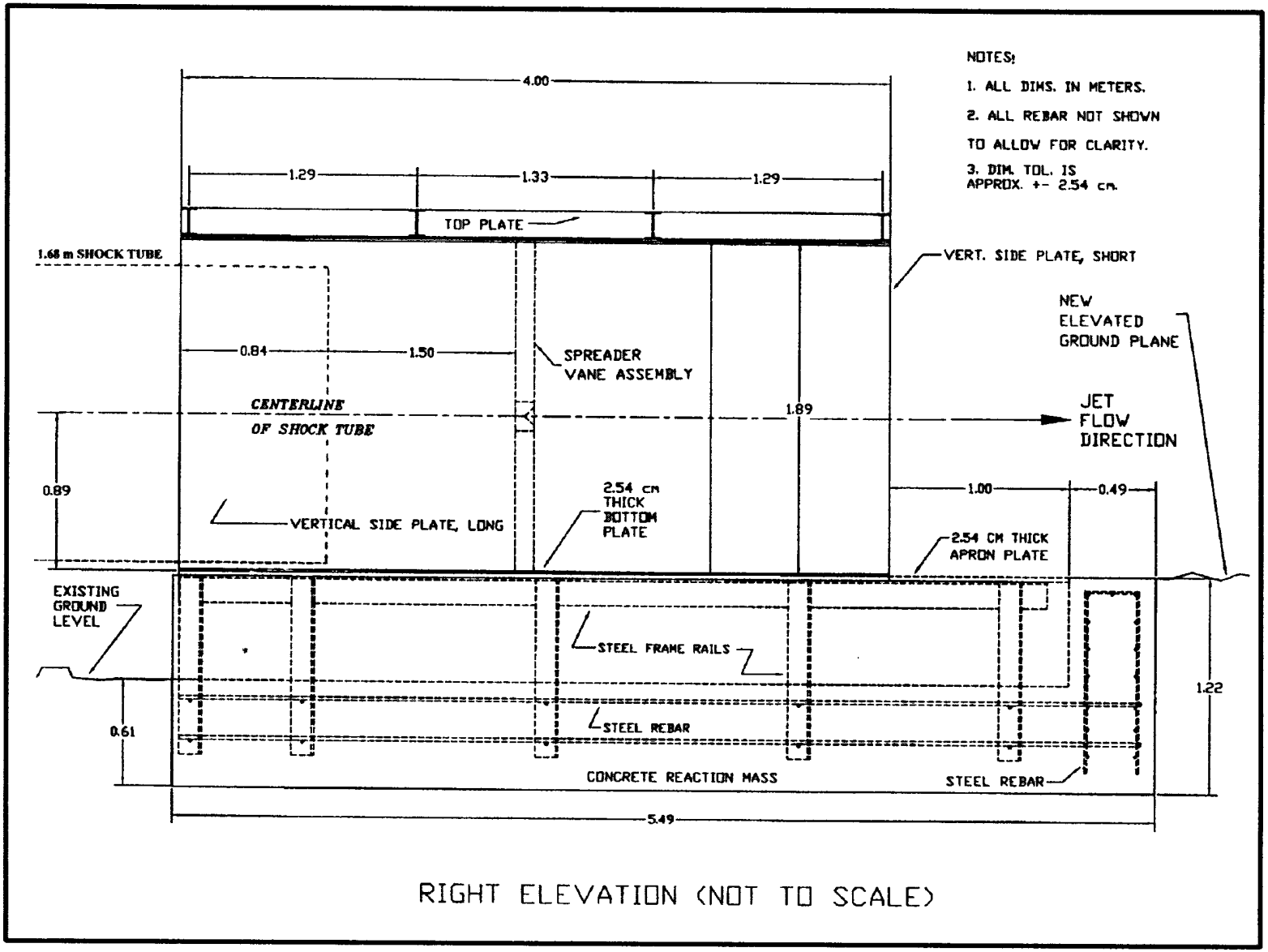

Figure 1. Right Elevation View of 1.68-m Shock Tube Exit Jet Spreader.

0.34 m on a perpendicular line from the shock tube axis. They span the entire height of the spreader. There is also a single, smaller, horizontal angle iron 7.62 cm (3.0 inches) on a side, 9.53-mm thick, with a 6.35-mm thick rib stiffener, placed halfway up the vertical angle irons and spanning the entire width of the spreader. The vertical location (at the height of the axis of the shock tube) of the horizontal spreader vane is also shown in Figure 1. These angle irons are hereinafter referred to as "spreader vanes." The vertical spreader vanes are designed to mechanically spread the exit jet laterally, with the two trailing edges of each vane continually shedding unstable vortex sheets to aid in the mixing of the already highly turbulent flow. The horizontal vane acts in the same way to perform a moderate amount of vertical spreading. As will be seen later, there was room for improvement in at least the positioning of the vanes, and possibly in the total number, but time and funding limitations did not permit further modification and testing.

Figure 2 shows a rear elevation view of the reaction mass and jet spreader, with the location of the 1.68-m shock tube exit overlaid upon it and the elevated ground plane indicated. The reinforced concrete reaction mass was designed to anchor the jet spreader at the end of the shock tube, doing so with no connection to either the shock tube or the shock tube's own reaction mass. The reinforced concrete (28-day, 31.0-MPa compressive strength) for the reaction mass was poured over a 15-cm thick base of crushed rock. The estimated friction coefficient for this combination of rock and soil was 0.44, indicating a horizontal holding force in shear on the bottom surface of 226.0 kN (50,700 lbf, where lbf denotes pounds force). An additional horizontal load-bearing capacity is derived from the front face of the concrete reaction mass that has a buried width and height of 4.47 m and 1.22 m, respectively, on its front face bearing against the elevated ground plane. The exact value of this load-bearing capacity is difficult to estimate. The safe bearing capacity for soft clay,[29] which is probably a worst case descriptor for the compacted soil in the elevated ground plane, is 0.10 MPa (14.5 psi). The context in which this number is given is such that it should be construed as applying only to a vertical load over a broad surface for laterally confined clay. If only the bottom fourth of the front face of the concrete reaction mass can be assumed to be acting efficiently against the soil, then this would imply a horizontal reaction force of the order of 136.3 kN (30,600 lbf). This component of the horizontal reaction force, which would only occur as a transient force during the flow time of the exit jet, can only be regarded as an estimate with probably a significant error bar associated with it.

Figure 3 shows a plan view of the jet spreader top plate, bottom plates, and reaction mass with the angled side walls removed for clarity. The exit plane of the shock tube is at the left in this view. Figure 4 shows details of the angled side plates, each of which consists of one long plate at the rear (i.e., entrance) of the jet spreader and one short plate positioned toward the exit of the spreader. The relative positions and angles of these two plates are seen in Figure 5, which is a plan view of the bottom plates, reaction mass, and angled side plates. All four of the side plates are set perpendicular to the bottom plates. The long side plates are angled outward 9 degrees relative to the shock tube axis to limit the maximum initial divergence angle of the exit jet, and the short side plates are set parallel to the shock tube axis to keep the exit jet from having an unconfined lateral expansion. The locations of the mounting holes in the top and bottom plates for the vertical spreader vanes, the side plates, and other components are also shown. Figure 6 shows another plan view that incorporates

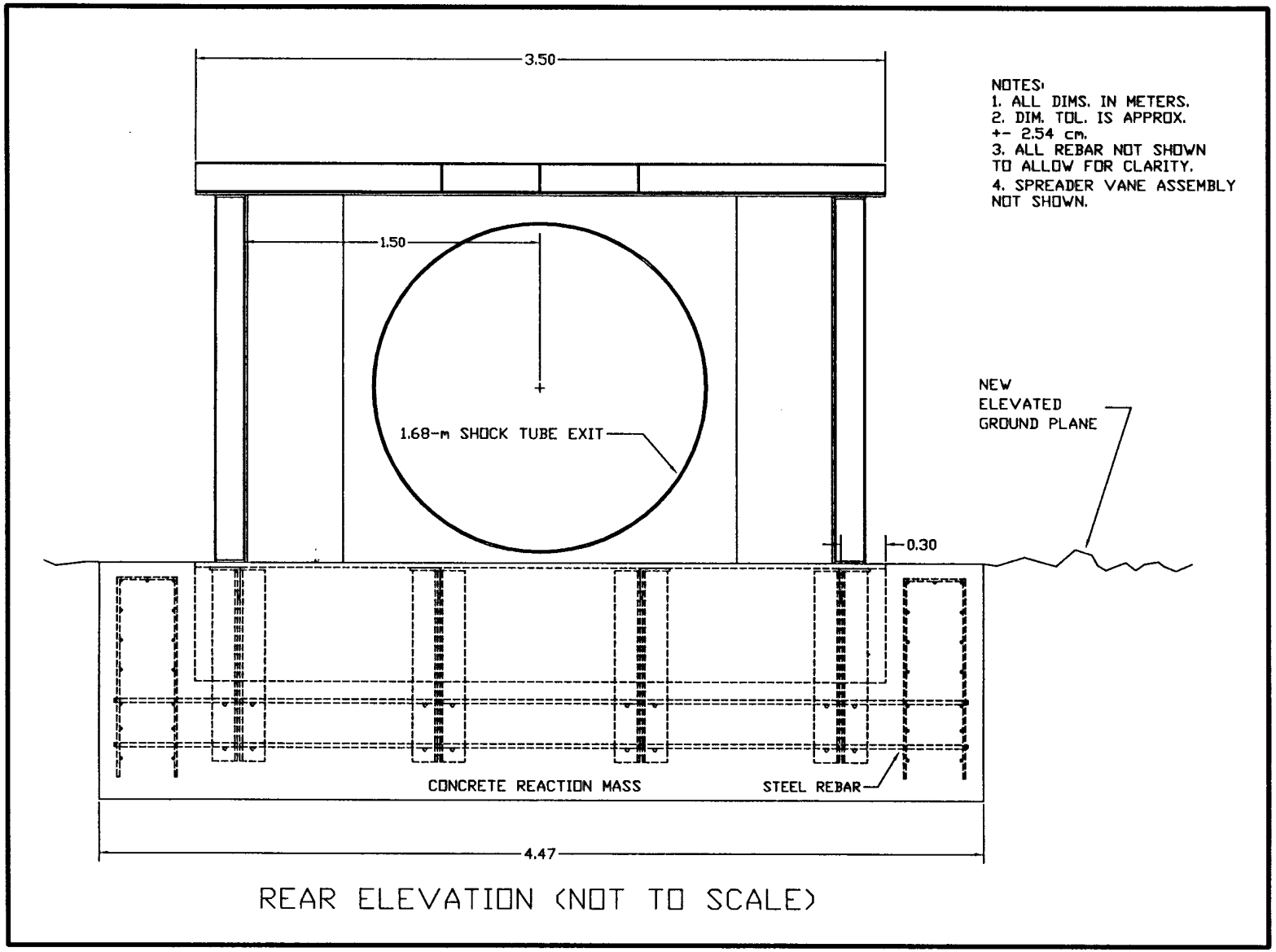

Figure 2. Rear Elevation View of 1.68-m Shock Tube Exit Jet Spreader.

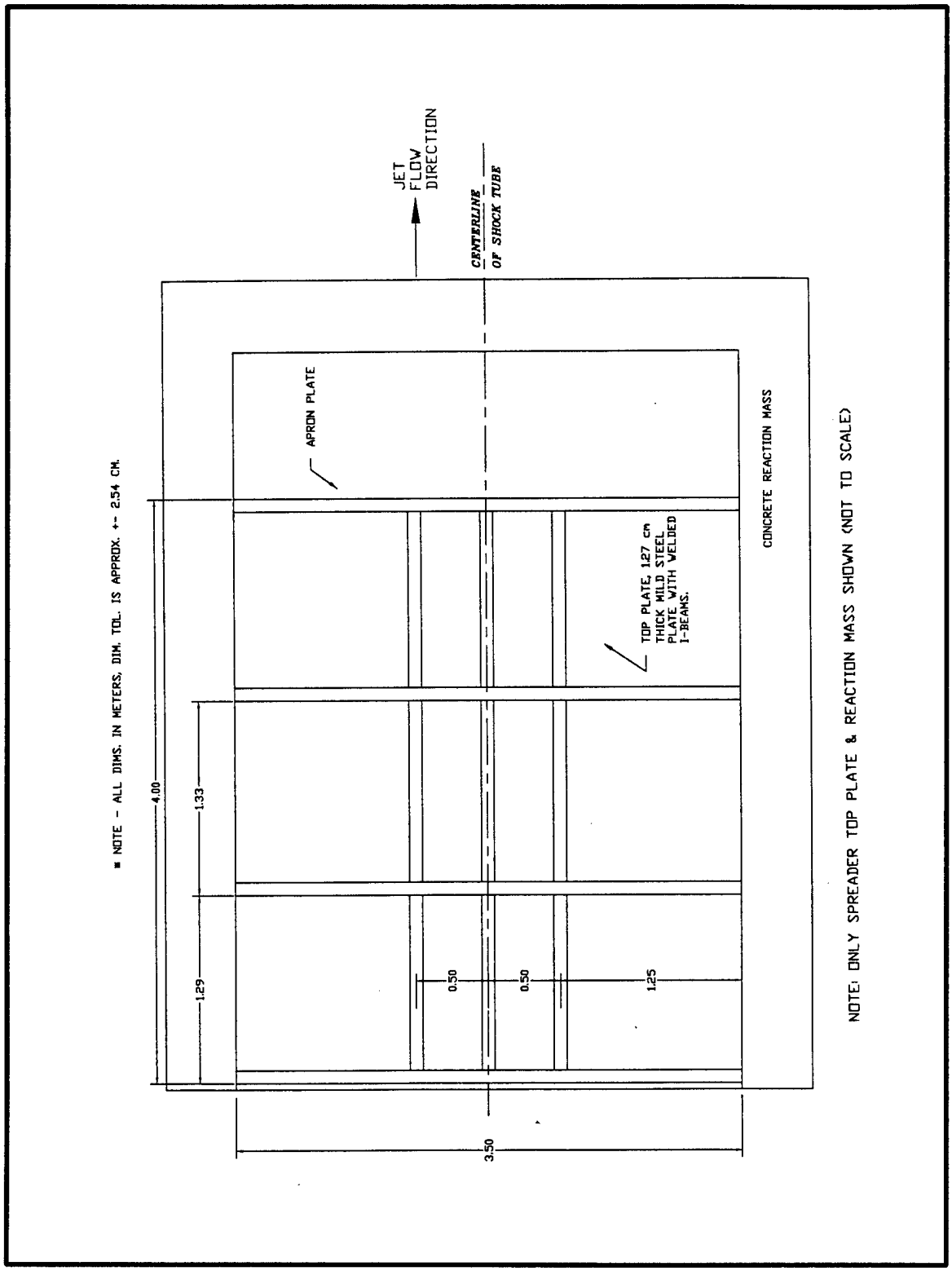

Figure 3. Plan View of 1.68-m Shock Tube Exit Jet Spreader.

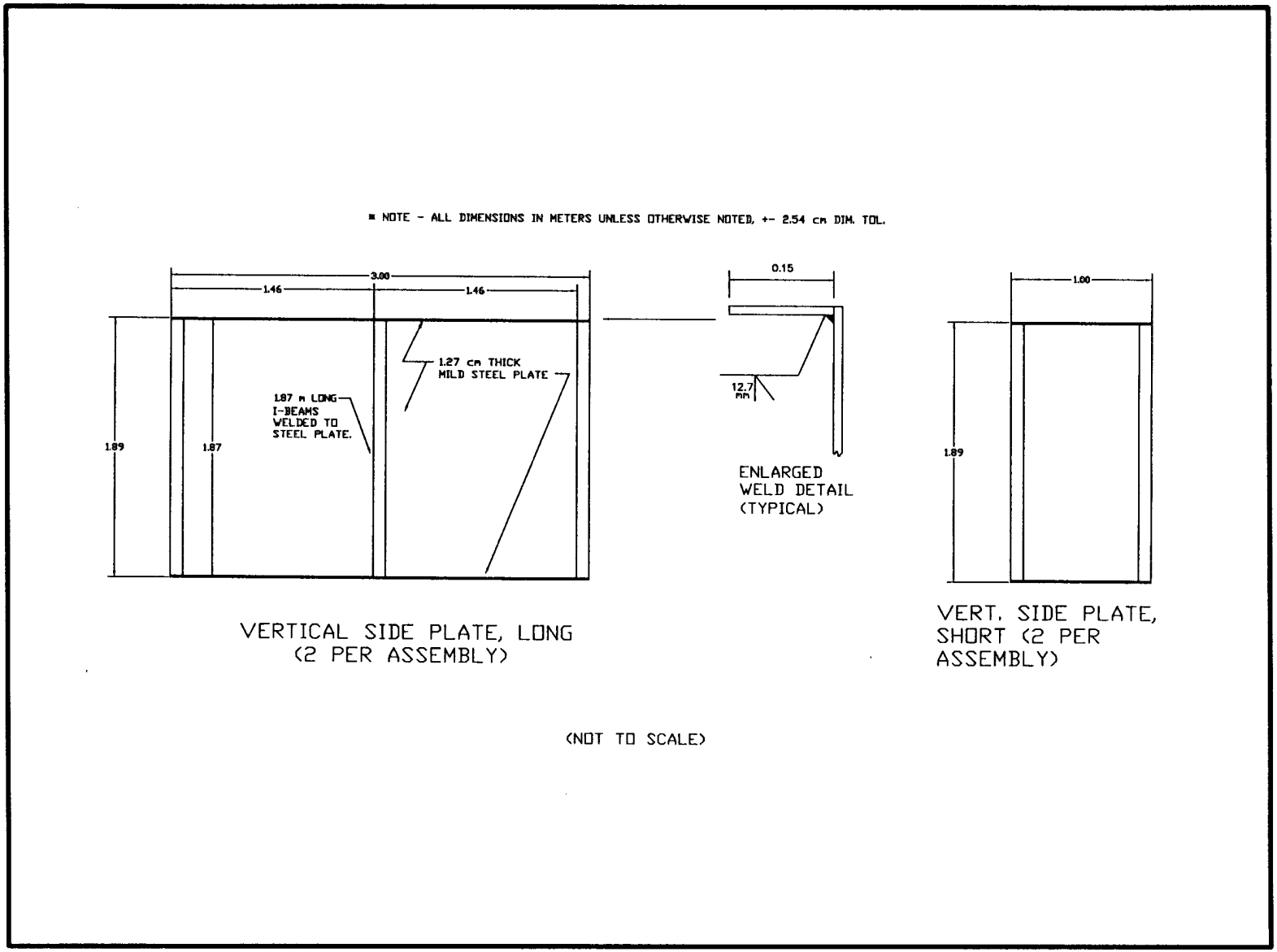

Figure 4. Detail Drawing for 1.68-m Shock Tube Exit Jet Spreader.

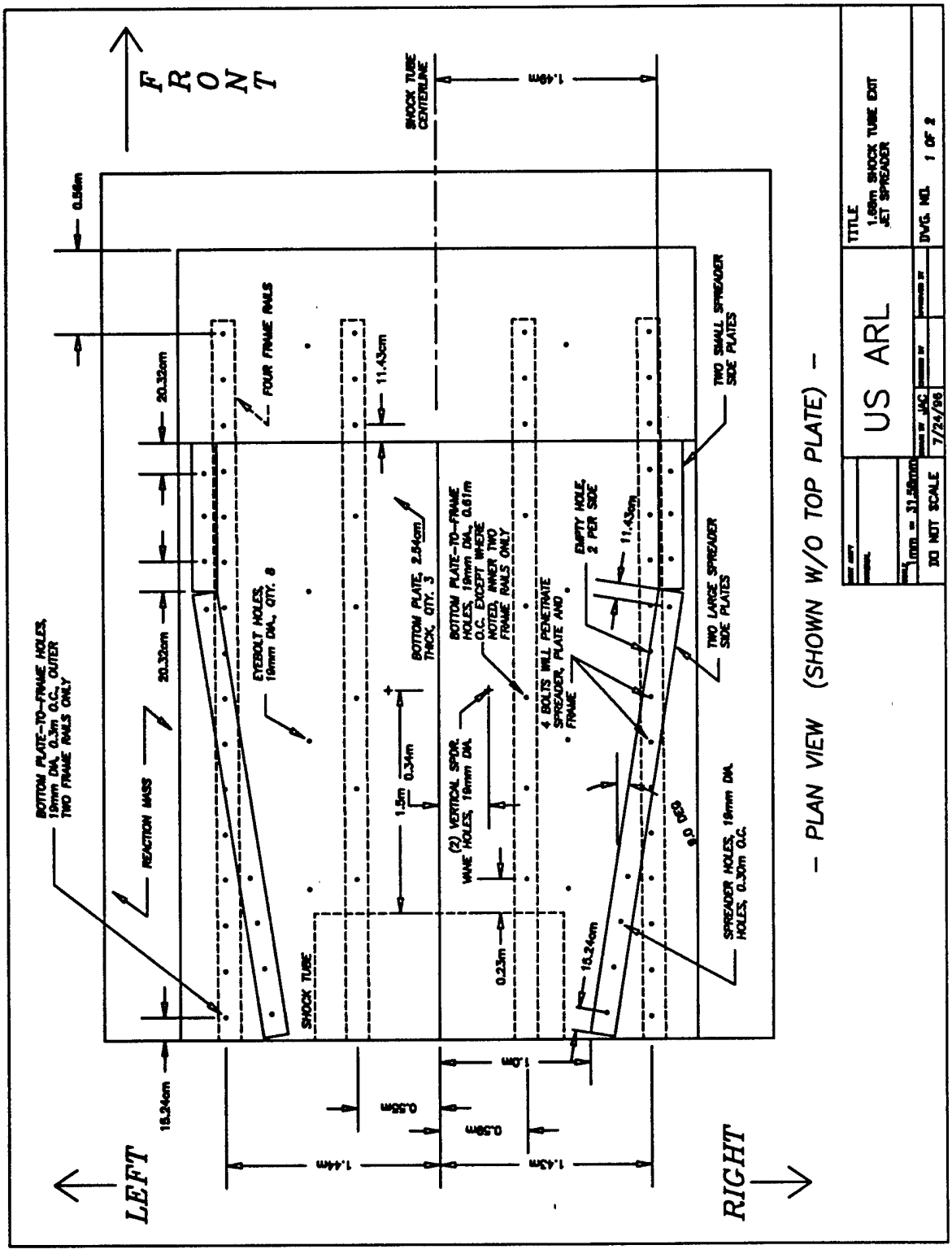

Figure 5. Assembly Details of 1.68-m Shock Tube Exit Jet Spreader, Sheet 1.

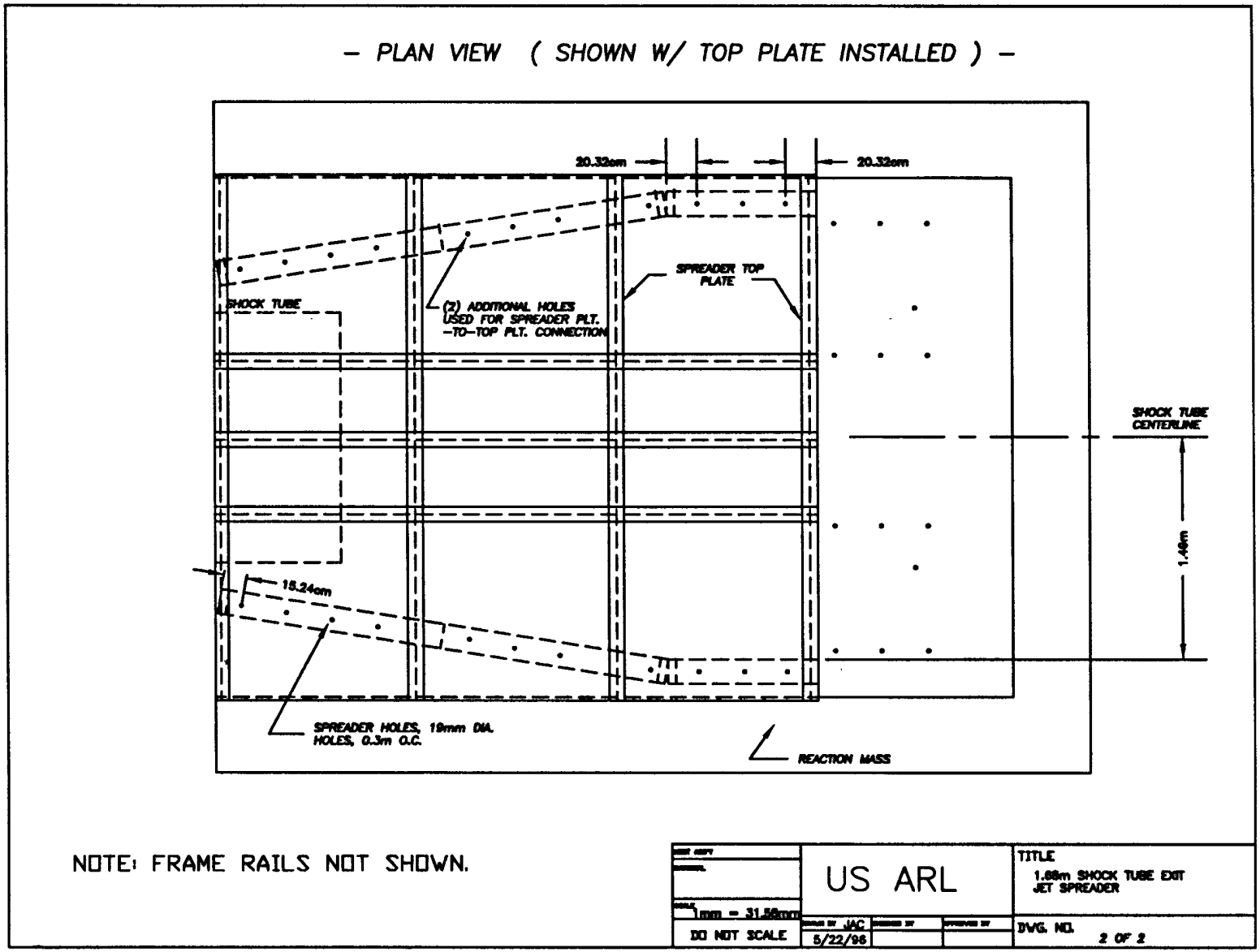

Figure 6. Assembly Details of 1.68–m Shock Tube Exit Jet Spreader, Sheet 2.

the top plate and its exterior stiffeners. The protruding end of the shock tube is also shown at the left in the figure.

A side view photograph of the finished exit jet spreader and elevated ground plane is shown in Figure 7. The assembled probe rakes and their temporary rolled homogeneous armor (RHA) mounting plate with its fixtures for attaching the rakes can be seen in the left of the figure. The original plan had been to put the two large concrete reaction masses with their mounting fixtures for the probe rakes that had been used in the unspread jet mapping studies back in place in the ground in the new, elevated ground plane, but time and funding did not permit that. The massive RHA plate with its mounting fixtures was used instead. The tips of the probes mounted in the rakes are located exactly at 10 shock tube diameters (16.76 m or 55.0 ft) downstream from the exit plane of the shock tube to match the primary reference location used in previous exit jet studies.[18] Figure 8 shows a photograph of the interior of the jet spreader as seen from the probe rakes, looking upstream toward the exit of the shock tube. The two vertical spreader vanes and single horizontal spreader vane are seen clearly in this view, as is the open area (i.e., entrainment area) around the shock tube at the rear of the jet spreader. This also gives a good indication of the bias toward lateral rather than vertical spreading on the jet that was designed into the jet spreader.

The finite element computer code ALGOR[30] was used in the structural design of the steel spreader and the steel spreader vane assembly. The loading for the jet spreader model used in ALGOR was conservatively based on an assumed shock static overpressure of 48.3 kPa to 103.4 kPa distributed normally over the interior surfaces of the spreader walls. The stress output results from ALGOR determined the choice of steel plate thickness and I-beam spacing to prevent material yielding in the final design.[18] Bolt spacings of 30.5 cm and 61.0 cm were used to attach the 2.54-cm thick steel apron and bottom plates to the steel frame rails of the reaction mass. The bolt spacing used to attach the four vertical side plates and top plate of the spreader to each other and to the steel bottom plate was approximately 30.5 cm. This spacing was derived by assuming a static overpressure of 103.4 kPa delivered normally to the exposed areas of the top horizontal plate and four vertical side plates, which resulted in force loadings distributed to the bolts in tension and shear, respectively. This design load required a minimum of seven Grade 5, 15.9-mm diameter bolts to be used to attach the vertical plates to the 2.54-cm thick bottom plate and to resist the shear loading from the static overpressure. For safety and convenience, 11 bolts were used on the top and bottom edges of each of the two vertical plate assemblies with an approximate 30.5-cm spacing on centers.

The spreader vanes were positioned within the jet spreader to force the flow to be distributed into a widened, more uniform pattern. Additionally, the generation of large vortex sheets from the trailing edges of the individual vanes aided in the kinetic energy transfers needed to promote a uniform spreading action. The vane geometry and configuration used in this testing was adapted from a successful earlier gas dynamic[17] and structural design.[18] The vane design used in this 1.68-m shock tube exit jet work is shown in detail in Figure 9. This relatively inexpensive and simple vane assembly consisted of the one horizontal and two vertical angle irons described earlier. These are scaled up from the earlier design which employed 5.08-cm wide by 6.0-mm thick angle iron for an intermediate scale exit jet spreader

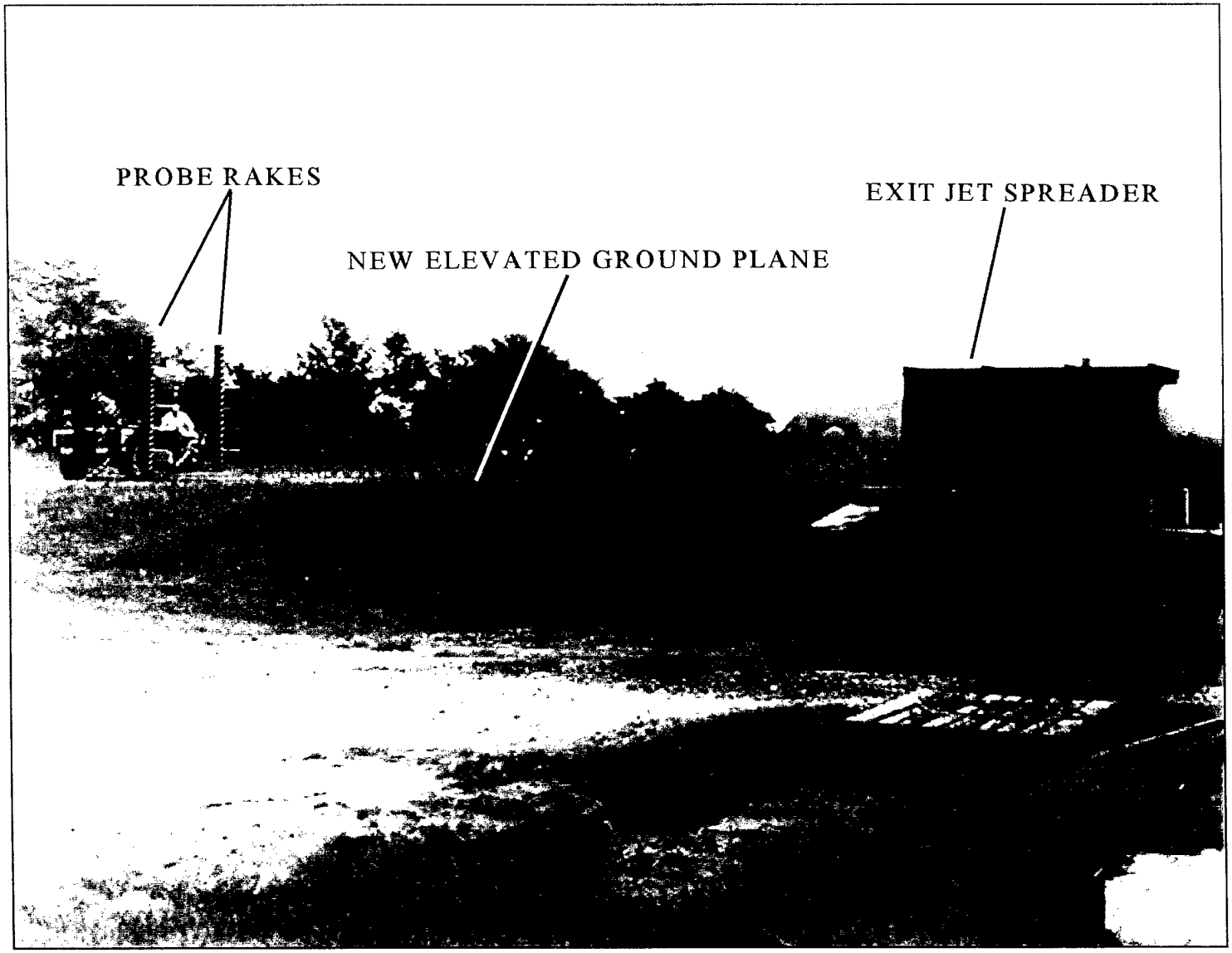

Figure 7. Side View of Completed 1.68-m Shock Tube Exit Jet Spreader Construction.

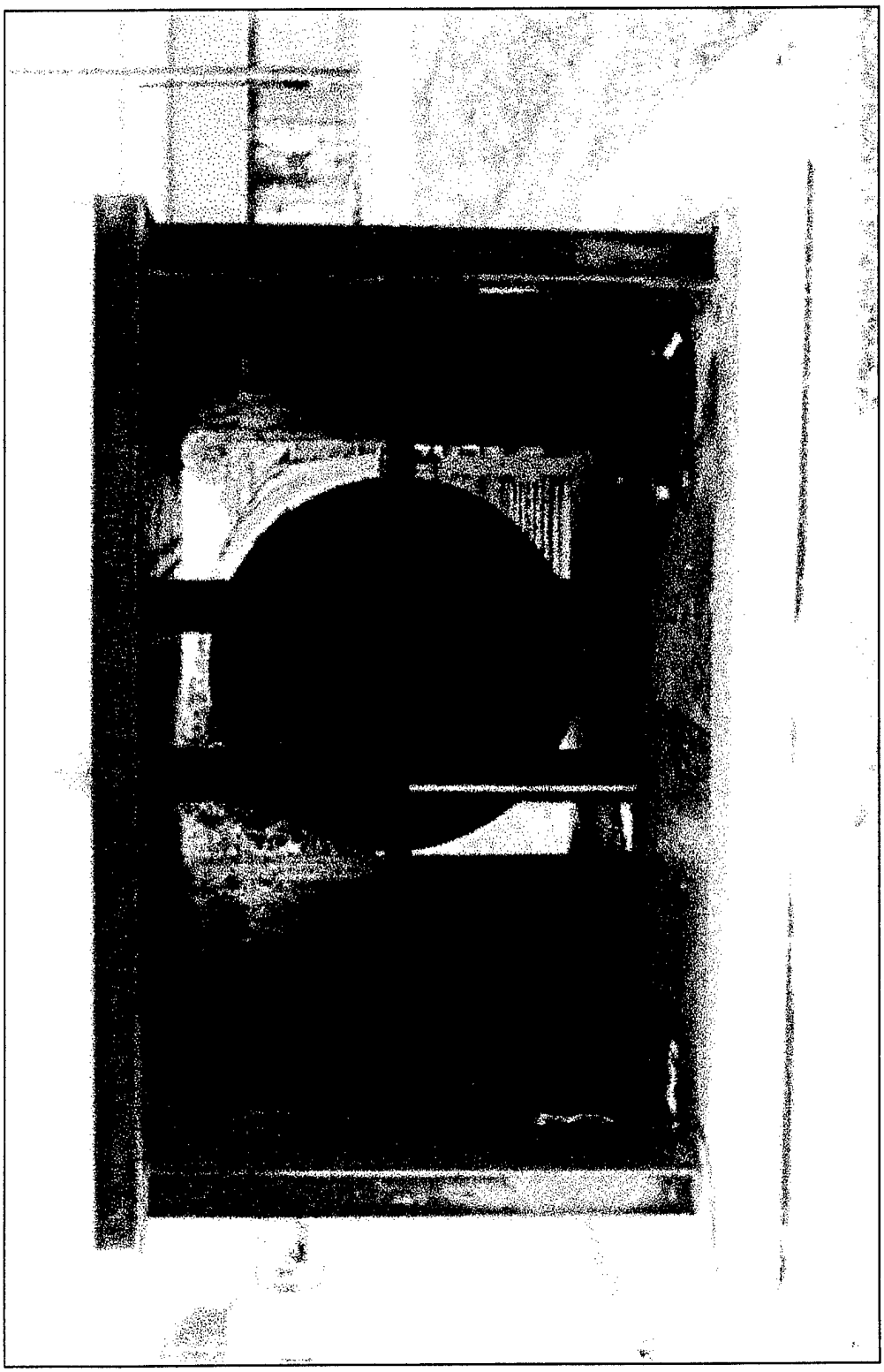

Figure 8. Rear View of Completed 1.68-m Shock Tube Exit Jet Spreader.

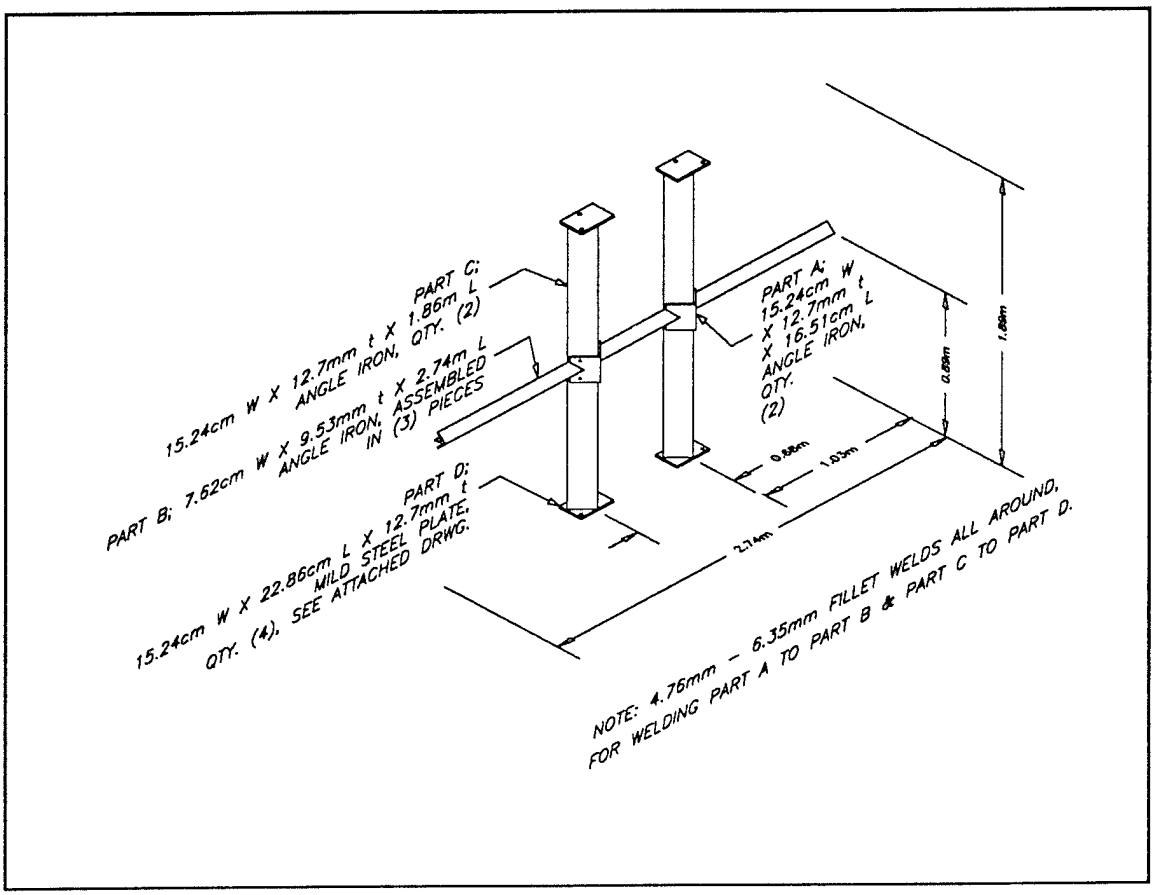

Figure 9. Spreader Vane Assembly for 1.68-m Shock Tube.

on the ARL 0.61-m diameter shock tube. The spreader vane structural design was modeled in ALGOR with shell elements and loaded with a conservative reflected pressure loading of 827.4 kPa (based on an assumed shock static overpressure of 137.9 kPa (20.0 psi), with a normally reflected overpressure of 413.7 kPa multiplied by a safety factor of 2.0) applied statically and normally to all upstream surfaces of the angle iron. The stress output results from ALGOR were used to qualitatively compare and optimize the structural integrity of the off-the-shelf angle iron, with and without 9.53-mm and 6.35-mm thick steel rib stiffeners, which would prevent yielding of the vane assembly under the applied pressure from the exit jet. The stress and displacement results from ALGOR are shown in Figure 10 (stress, without stiffeners), Figure 11 (displacement, without stiffeners), Figure 12 (stress, with stiffeners), and Figure 13 (displacement, with stiffeners). In these figures only half of the vane assembly is modeled because of symmetry. These results show that by simply welding stiffeners to the downstream side of the angle iron, stresses could be reduced by approximately 50 percent and still allow for the vane components to be manually positioned and bolted inside the spreader. In the actual construction, Grade 5, 15.9-mm diameter bolts were used to fasten the vane assembly to the top, bottom, and side plates of the spreader. However, bolts were not modeled in the structural analysis, and model nodes that were coincident with the angle iron-to-spreader plate connection areas were modeled as being totally fixed in the global coordinate system. Linear material properties were used for simplicity.

3. INSTRUMENTATION AND TEST DATA

Two 2.59-m high steel probe rakes were used to position pressure transducer instrumentation (three to four probes per rake), mounted as described earlier to an RHA base plate within the spread exit jet at a standoff distance of 10 shock tube diameters, or 16.76 m, from the end of the shock tube exit jet plane (see Figure 7). A side view photograph of the probe rakes, giving a good view of the vertical spacing of the mounts for the pressure probes, is shown in Figure 14. The second probe from the bottom is at the height of the axis of symmetry of the shock tube. Figure 15 shows a plan view of the base plate. One probe rake was mounted at the zero radius position, directly on line with the axis of symmetry of the shock tube. The second probe rake was mounted at the $3r$ position, which was at a radial distance equal to three shock tube radii. Each probe had a stagnation and a static (i.e., side-on) pressure transducer. The probe rake steel base was designed in such a way as to allow relatively easy repositioning of the probe rakes at 0, 1, 2, and 3 shock tube radii, without requiring repositioning of the 3.94-Mg base plate itself. In this study, only the 0 and 3 shock tube radii positions were used. The base plate also had to resist the overturning moment created by the drag loading of the probe rakes within the spread jet. The details of the mounts on the probe rake base plate are shown in Figure 15.

Differential pressure and differential pressure impulse data, computed in the same manner as Kingery and Gion[11] and Bryant and Allen,[2] were acquired from this instrumentation for each test. As a sample, a four plot set of digitized data for the third probe up from the ground (second probe from the top) on the probe rake on the shock tube centerline is shown in Figure 16. The upper left plot is the stagnation overpressure; the upper right plot is the

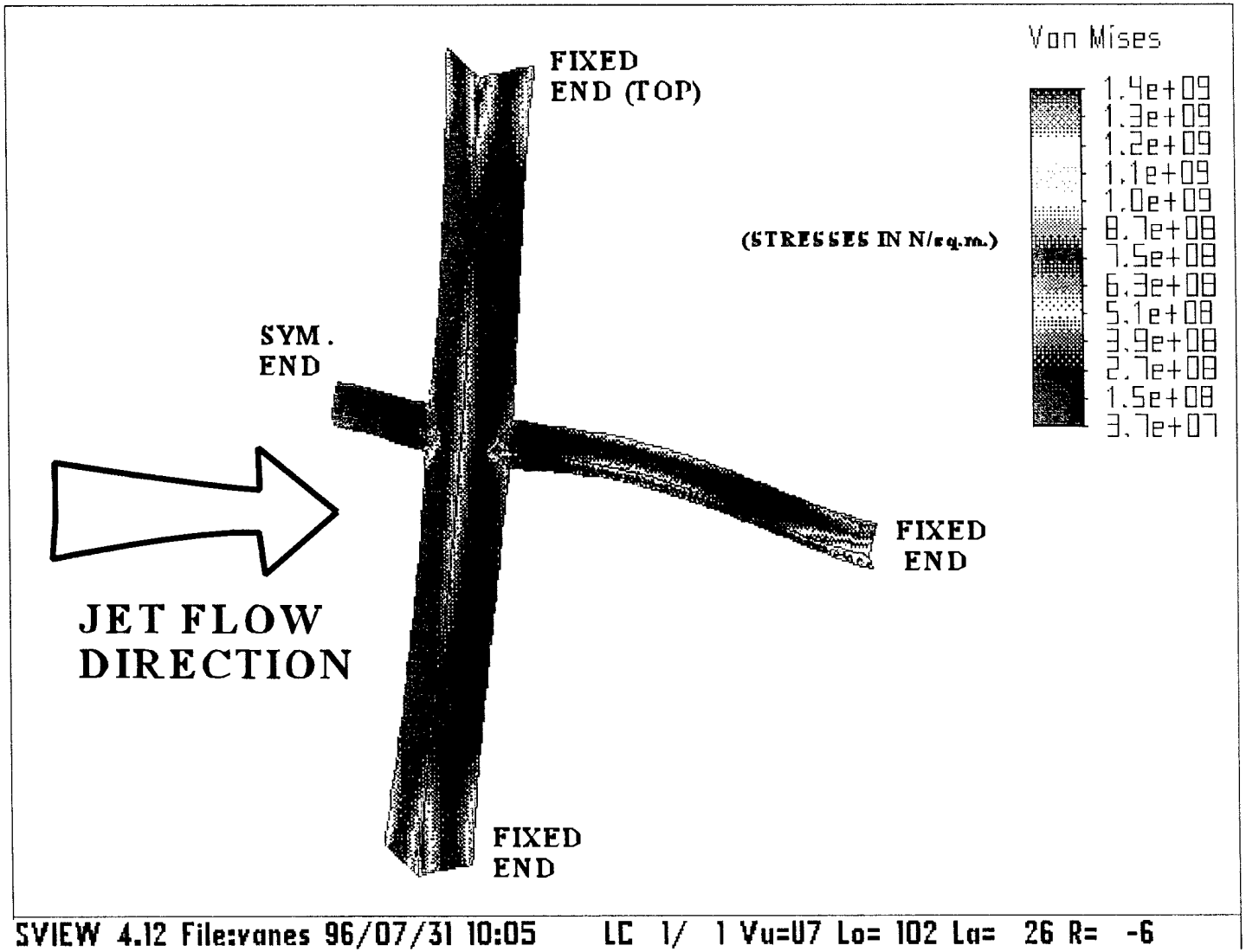

Figure 10. ALGOR Stress Results of Half Symmetry Spreader Vane Assembly Without Stiffeners.

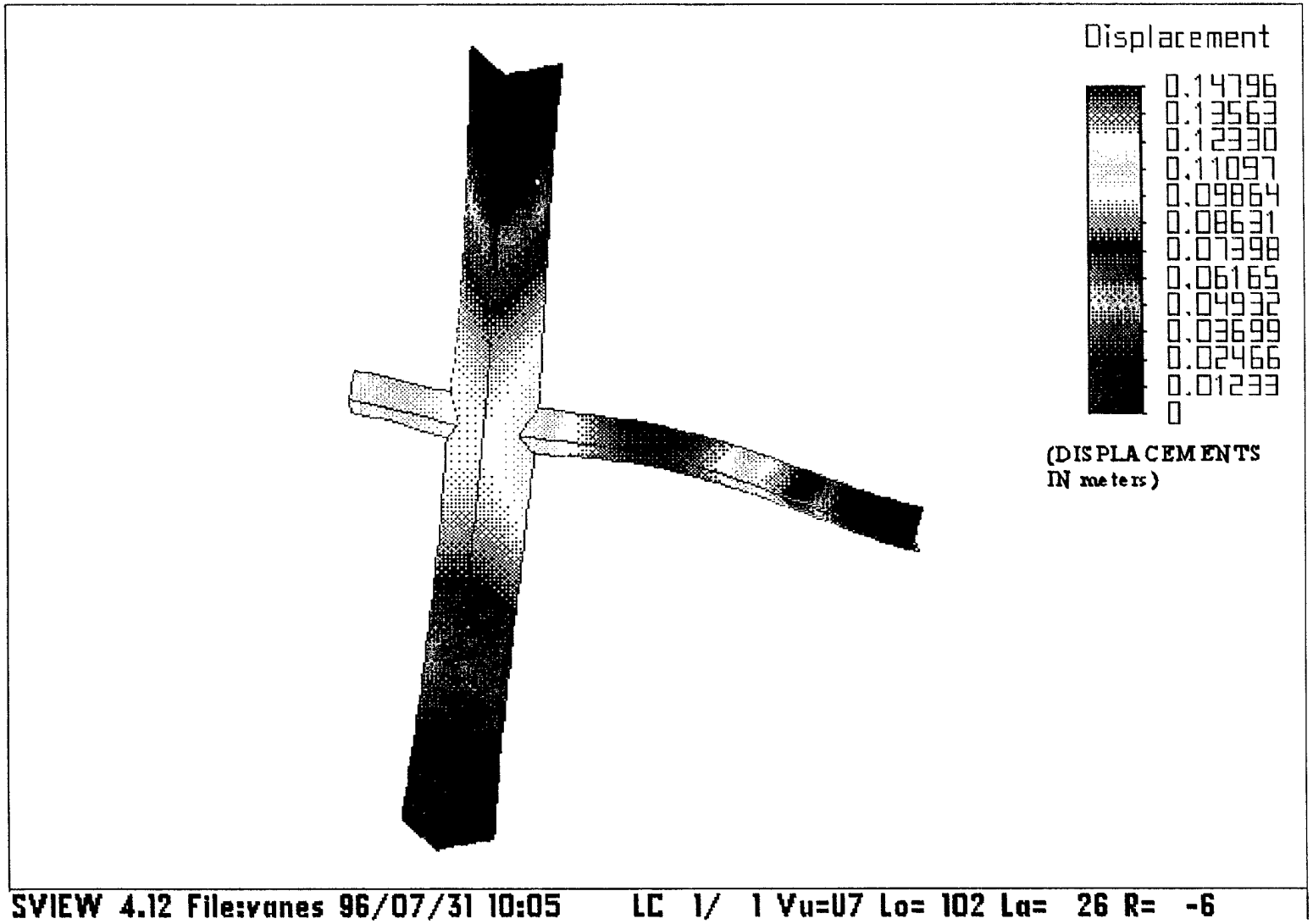

Figure 11. ALGOR Displacement Results of Half Symmetry Spreader Vane Assembly Without Stiffeners.

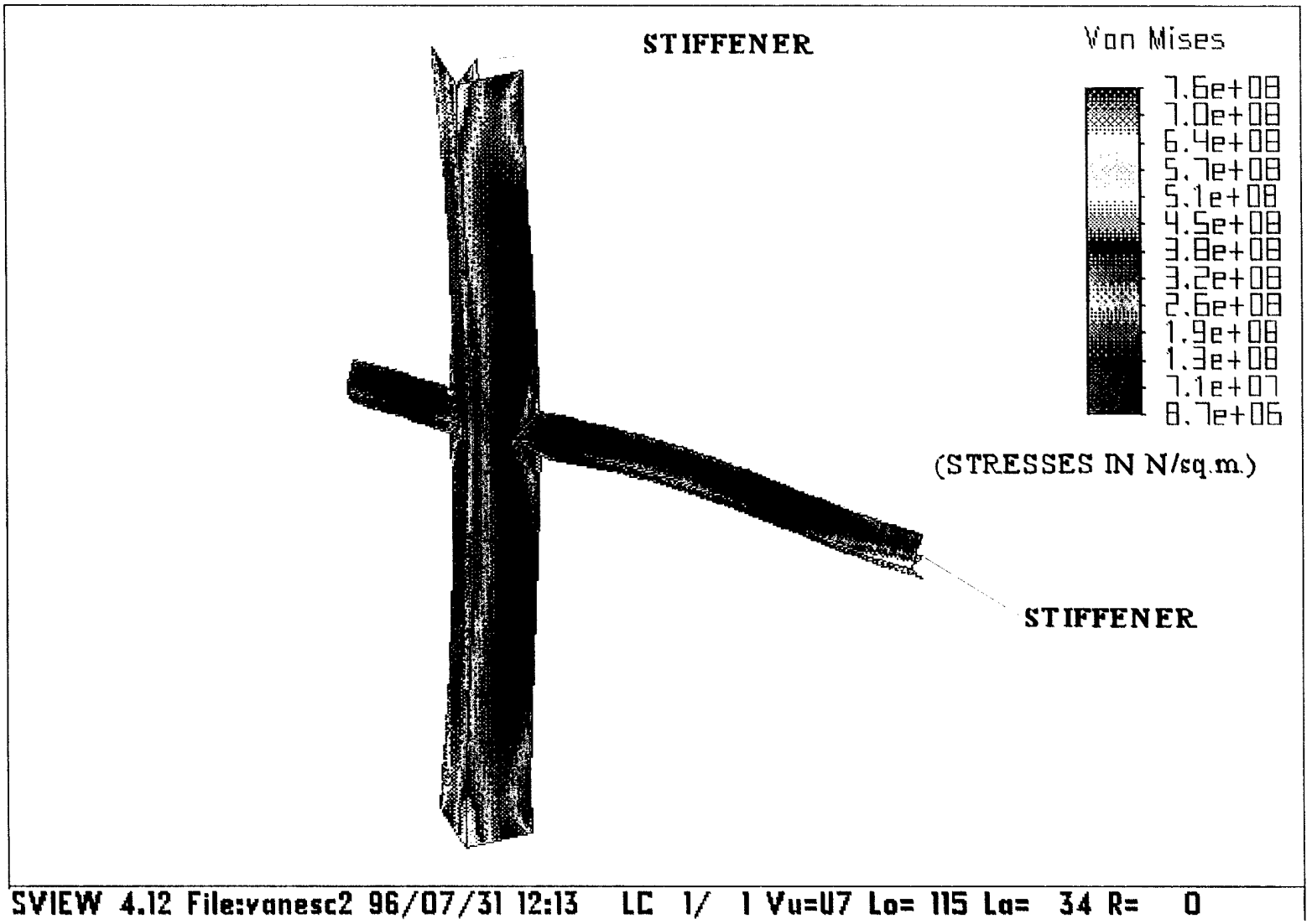

Figure 12. ALGOR Stress Results of Half Symmetry Spreader Vane Assembly With Stiffeners.

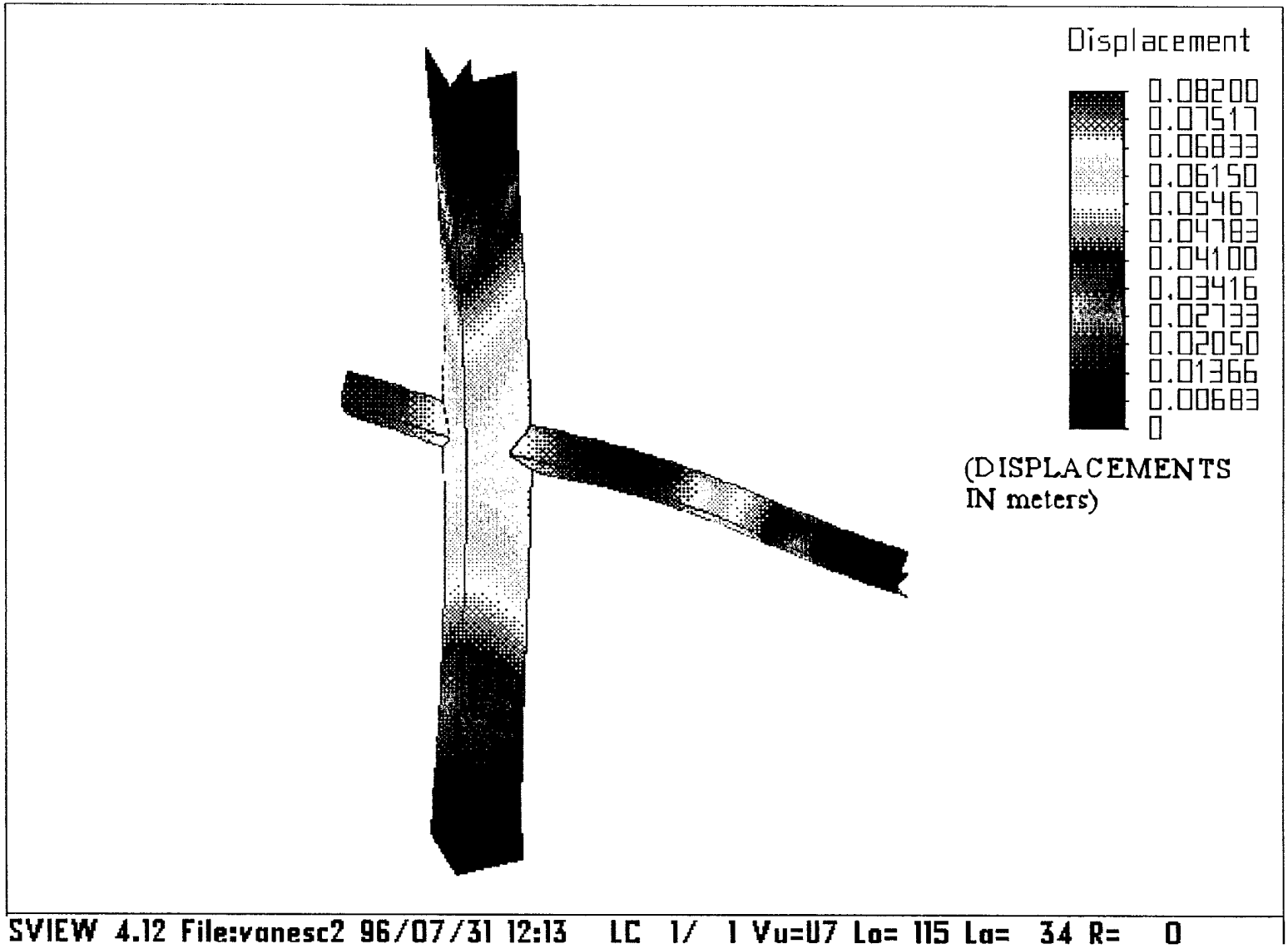

Figure 13. ALGOR Displacement Results of Half Symmetry Spreader Vane Assembly With Stiffeners.

Figure 14. Side View of Pressure Probe Rakes and Base Plate.

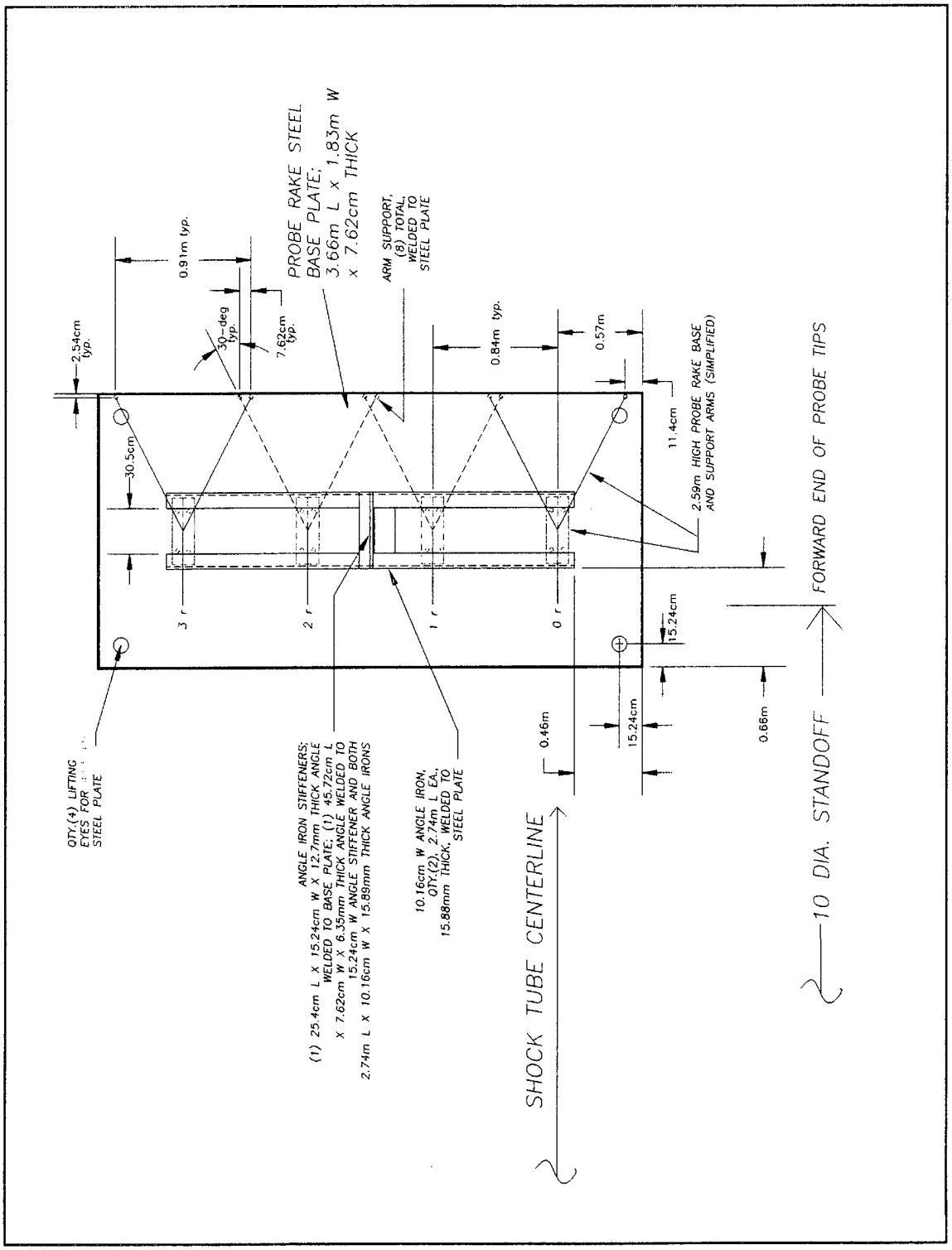

Figure 15. Plan View of Probe Rake Base Plate.

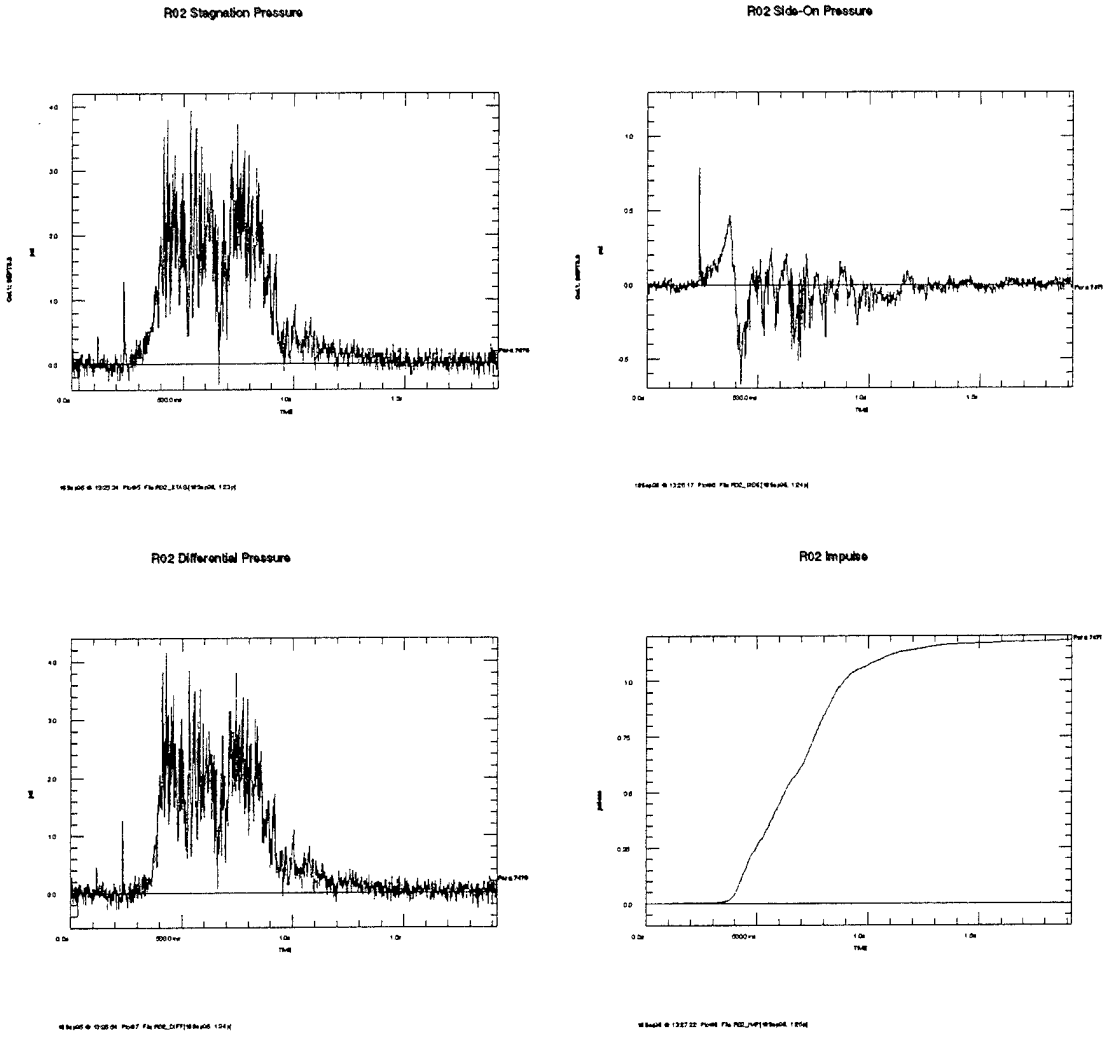

Figure 16. Typical Pressure Probe Rake Digitized Data (Probe R02 for Test 1 shown).

static overpressure; the lower left plot is the pressure difference (stagnation minus static); and the lower right plot is the integral over time of the impulse from the pressure differential, here representing the differential pressure impulse in the same manner as described previously.

In addition to the pressure probe instrumentation, metal cubes, 5.08 cm on a side, were positioned[31] on raised metal spikes along the ground at various diameters from the exit jet. The cubes, some of aluminum and some of steel, were oriented with their centers of gravity approximately 12.7 cm above ground level. These cubes were used as a second method of indirectly determining dynamic pressure impulse from maximum total displacement (i.e., the vector sum of the axial plus radial displacement) and qualitatively determining the effectiveness of the spreader and vane configuration. Past testing with these same cubes in high explosive environments (e.g., an ammonium nitrate/fuel oil high explosive test DISTANT IMAGE[32]) allowed for relationships to be derived which relate their displacement to the dynamic pressure impulse delivered by a blast wave. The relations[31] are, for the steel cubes,

$$(I_q)_{FE} = 2.0D^{0.4}, \tag{3}$$

and for the aluminum cubes,

$$(I_q)_{AL} = 0.73D^{0.48}, \tag{4}$$

in which the dynamic pressure impulse is given in kPa-s and the displacement, D, is in meters.

4. TEST PLAN

Shock tube driver pressures were selected which would result in specific impulse loads of approximately 1.0 kPa-s to 4.0 kPa-s delivered to a target vehicle placed at the 10-diameter standoff position. This impulse range was chosen to further investigate the relationship of total horizontal displacement of Army jeep vehicles and delivered horizontal dynamic pressure impulse. Past studies[33] on WWII M151A2 type jeeps during earlier nuclear and high explosive tests compared their displacements with delivered differential pressure impulse and were used as a guideline. These data indicated that for this specific impulse range, the jeep displacements would range from 1.0 m to 10.0 m. In addition, past research data,[18] which correlated driver pressures of the unspread jets from the 1.68-m and 10.16-cm shock tubes with delivered differential pressure impulse at the 10-diameter standoff position, were used in selecting the corresponding 1.68-m shock tube driver pressures for the spread jet. With the intention of testing these same type jeeps with the spread jet from the 1.68-m shock tube, the 1.0-kPa-s to 4.0-kPa-s impulse range was finally chosen in light of the physical constraints of the test range which only allowed for approximately 12.0 m of level ground beyond the 10-diameter location of the probe rakes. The research plan allowed for a total of five tests. All five tests were instrumented with the probe rakes at the 10-diameter axial position (one at the shock tube centerline, or zero radius, and one at three radii) and the metal cubes were positioned in rows at the 10-, 13-, and sometimes the 15-diameter range. The total number of metal cubes used in each test varied. A typical cube-positioning configuration is shown in

Figure 17. Metal Cube Displacement at 10-Diameter Axial Range for Test 3.

Table 1. Test Conditions.

Test Number	Date (1996)	Driver Gauge Pressure (kPa)	Test Conditions and Configuration
1	3 Sep	289.6	Temp: 80's (degrees F) Humid Dry Ground Plane Pressure Probes; Cubes
2	4 Sep	172.4	Temp: 80's (degrees F) Humid Dry Ground Plane Pressure Probes; Cubes
3	9 Sep	137.9	Temp: 80's (degrees F) Humid Dry Ground Plane Pressure Probes; Cubes
4	10 Sep	158.6	Temp: 80's (degrees F) Humid Dry Ground Plane Jeep Target Pressure Probes; Cubes
5	12 Sep	144.8	Temp: 80's (degrees F) Humid Muddy Ground Plane Jeep Target Pressure Probes; Cubes

the photograph of the mounting pins and scattered cubes in Figure 17. The mounting pins are still in their original, pretest positions, and the cubes are in their untouched post-test positions. The first three tests provided jet mapping data and verification of the anticipated differential pressure impulse values. Metal cubes were fielded in these tests, but no jeeps were included. The fourth test was conducted with the jeep positioned so that its center of gravity was coincident with the shock tube's centerline (probe rake $0r$). The upstream faces of the tires were 1.57 m (62 inches, approximately one diameter) downstream from the 10-diameter location of the tips of the probe rakes (see Figure 18). Metal cubes were used in this test but had not yet been positioned at the time of the photograph. Not all metal cube positions were used because of the presence of the jeep. The fifth and final test was conducted with the jeep positioned so that the shock tube's centerline was aligned with the jeep's estimated center of area (see Figure 19). In this test, the upstream faces of the tires were 1.47 m (58 inches) downstream from the tips of the probe rakes. As with Test 4, a reduced number of metal cubes were also included in Test 5. Table 1 shows details of the testing with required shock tube driver pressures and conditions.

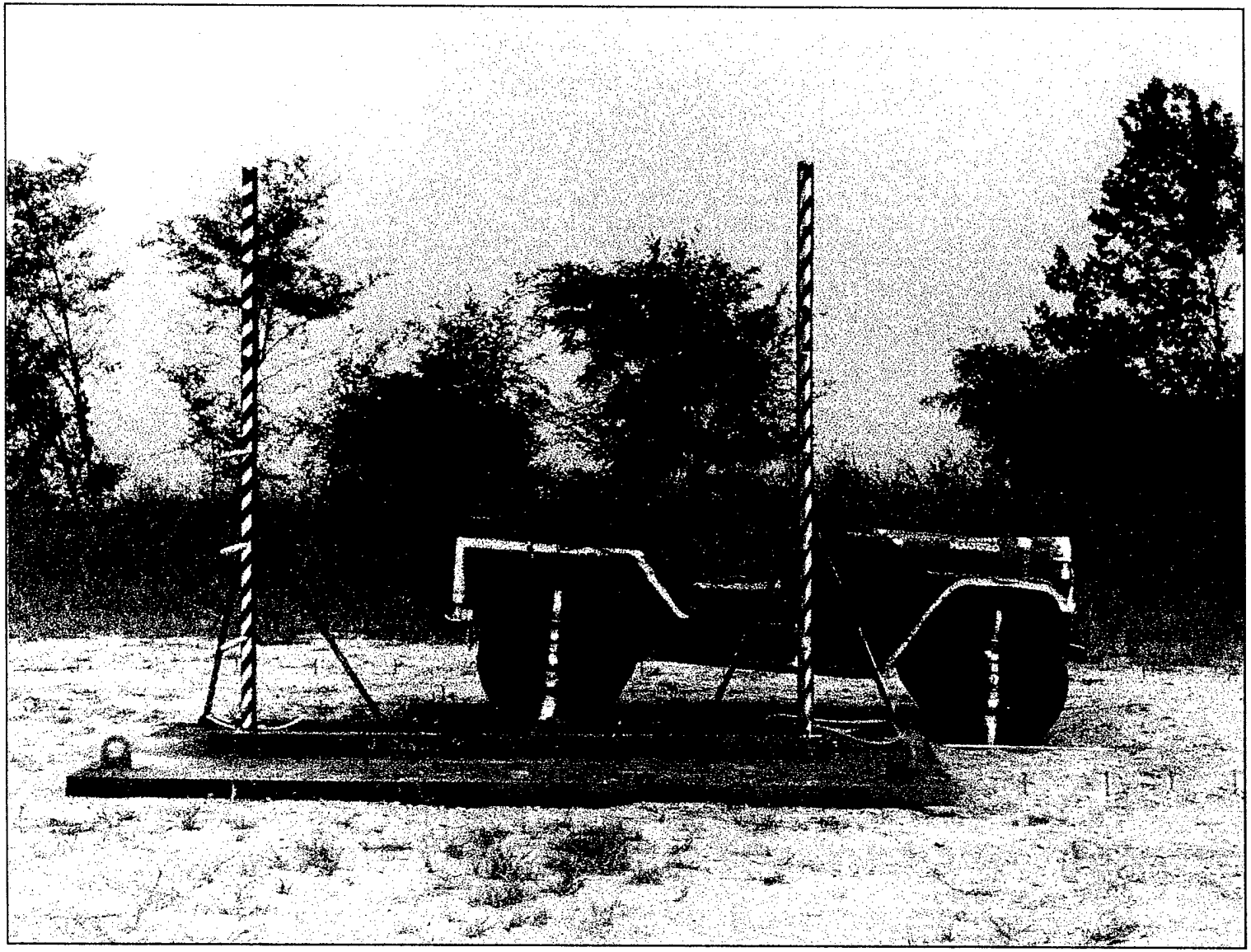

Figure 18. Jeep Initial Position in Test 4.

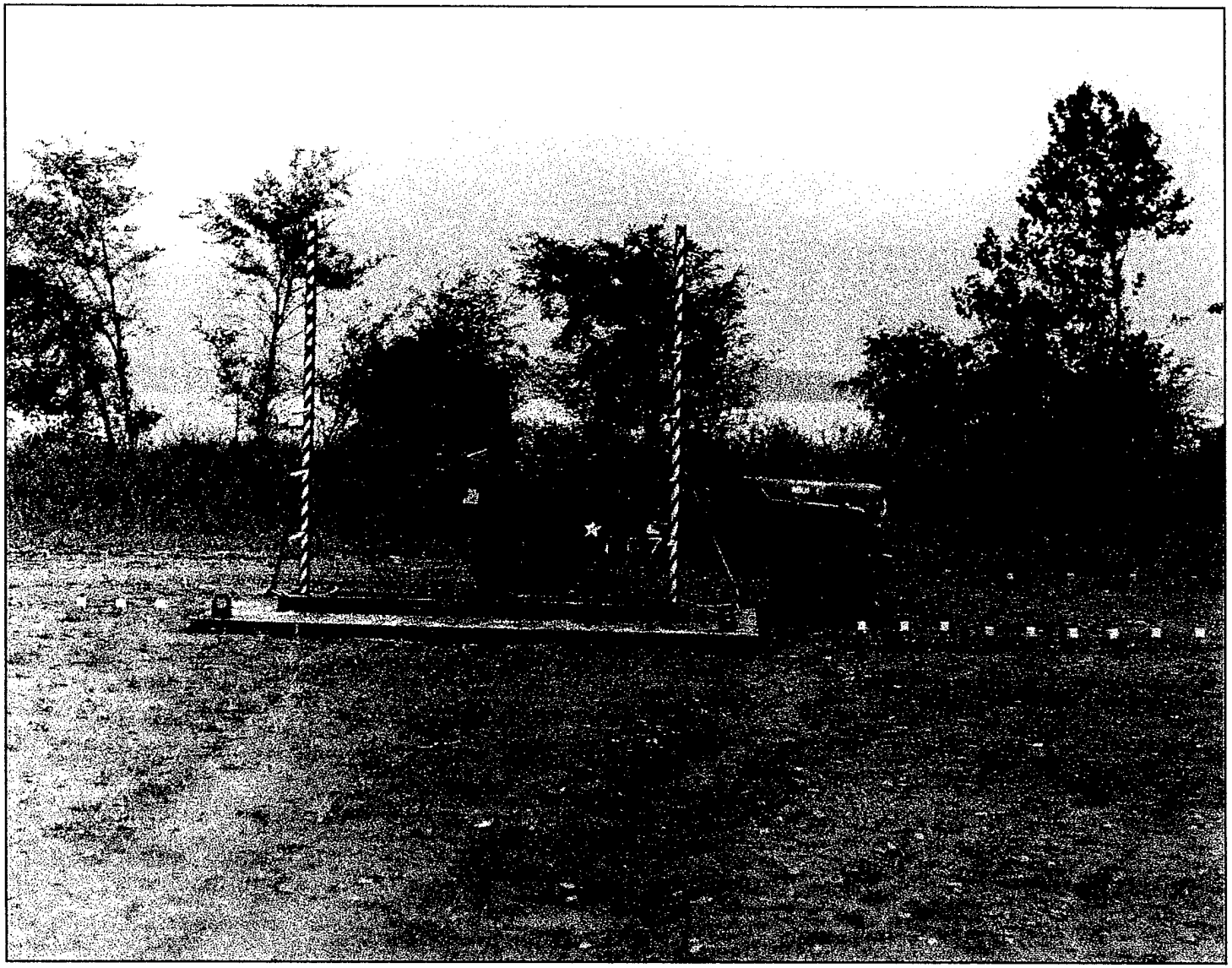

Figure 19. Jeep Initial Position in Test 5.

5. Test Results

Averaged differential pressure impulse versus driver pressure results are shown in the plot in Figure 20. Before the discussion of the results, some definition of terminology is in order. The left probe rake is defined as the one positioned at the $3r$, or three shock tube radii from the center line, location as viewed by an observer facing toward the probe rake assembly and away from the shock tube exit. The probe positions are numbered from the top to the bottom, with a leading letter to indicate which probe rake is being discussed. Thus, the highest probe on the left, or $3r$, rake, is $L01$, the next down the left rake is $L02$, and so on. Similarly, the centerline probe rake, being toward the right from that same perspective, has probe numbers $R01$ (at the top) through $R04$ (at the bottom). In this plot, the impulse data for each of the pressure probes on the left ($L01$ through $L03$), or $3r$ probe rake, and the right ($R01$ through $R04$), or $0r$ probe rake, were averaged. In addition, impulse data were averaged for the three to five cubes that were placed at the 10-diameter location, at the $1.5r$ to $2.7r$ range, for each test. Linear curve fits or regressions were performed to indicate the trends of differential pressure impulse versus driver gauge pressure for the probe rakes and cubes. From this plot, it can be said that the centerline probe data agree fairly well with the cube data. However, because of the results from the $3r$ probe rake also shown in Figure 20, it looks as though the spreading action of the jet is not totally uniform but is approximately at 50 percent strength at this off-center location. (The unspread, highly collimated shock tube exit jets experience an even greater reduction at this location.) Thus, it appears that the spreader vane locations, and possibly number of vanes, were effective but not yet optimized for the 1.68-m shock tube. Time and funding limitations precluded further work to do this optimization.

Differential pressure impulse versus radial distance within the exit jet are shown in the plots in the next several figures. Figure 21 shows the results from Test 1, which had a driver gauge pressure of 289.6 kPa (42.0 psi). There is a fairly symmetric, sharp drop-off in differential pressure impulse between two and four radii, with good agreement among the various measuring methods. The cubes at the 10-diameter position are the closest to the pressure probe axial position and show good agreement. The differential pressure impulse inferred from the cubes is based on the total vector displacement of the cubes from their original positions, as described before. This was a relatively strong jet, with some cubes displaced into an earthen berm at the end of the raised ground plane, thereby invalidating their displacement data. Those cubes were not included in this plot. This test delivered a differential pressure impulse of approximately 4.25 kPa-s (averaged $0r$ probe rake data plus cubes near the shock tube centerline), somewhat beyond the high end of the desired range of impulse delivery for the planned jeep displacement tests. Figure 22 shows the results for Test 2, which had a reduced driver gauge pressure of 172.4 kPa (25.0 psi). This showed more scatter in the data, with the averaged $0r$ probe rake data being the highest at approximately 3.6 kPa-s. This may be because the cubes were influenced by a boundary layer effect (not seen by the higher probes in the rakes), by a too-low set of static pressure gauge readings, by a shadowing of the cubes by the protruding 7.62-cm thick base plate, or by some other effect. Figure 23 shows the results for Test 3, which had the driver gauge pressure further reduced to 137.9 kPa (20.0 psi). This jet did not show as good symmetry as the two stronger

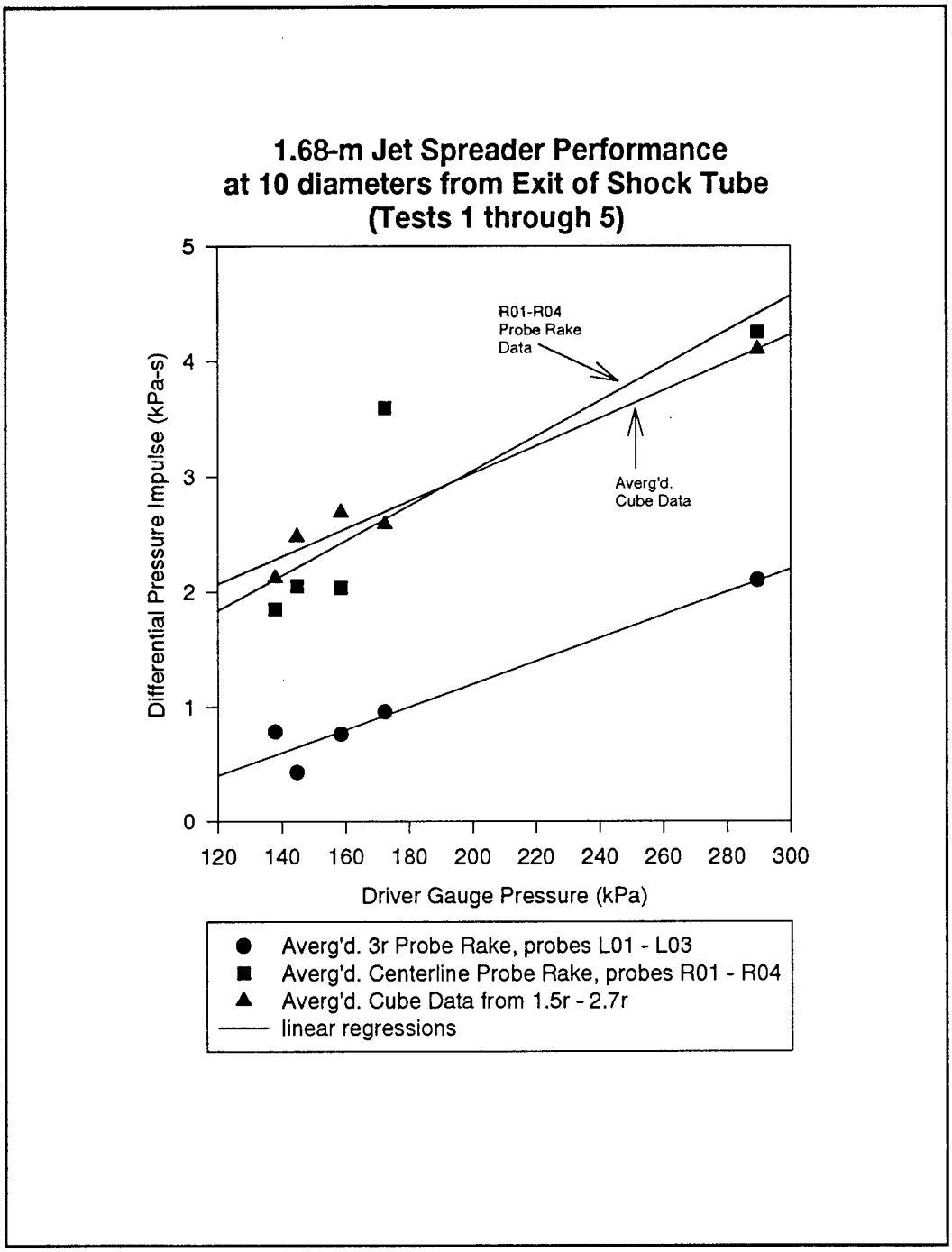

Figure 20. Differential Pressure Impulse Versus Driver Gauge Pressure.

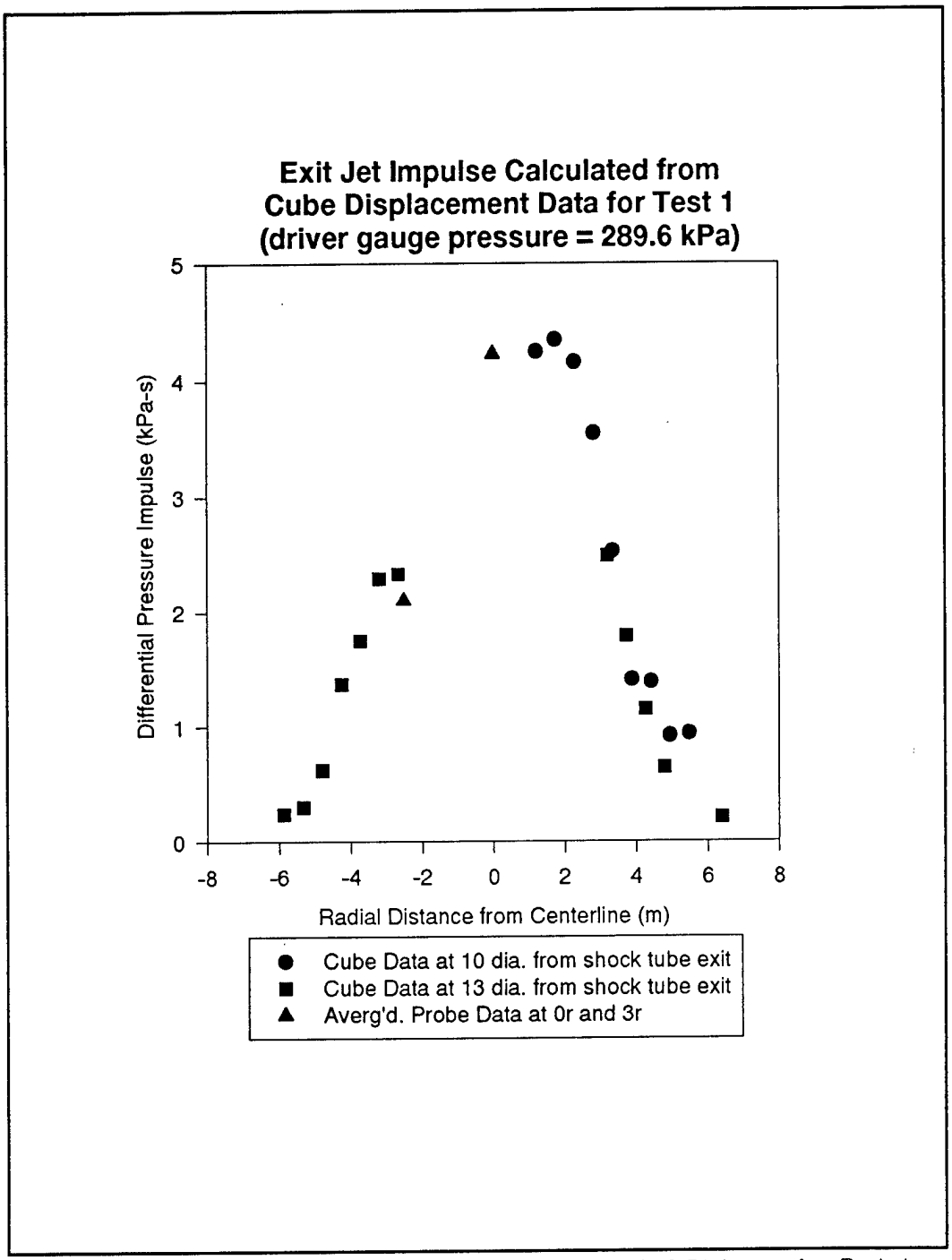

Figure 21. Differential Pressure Impulse Versus Radial Distance for Test 1.

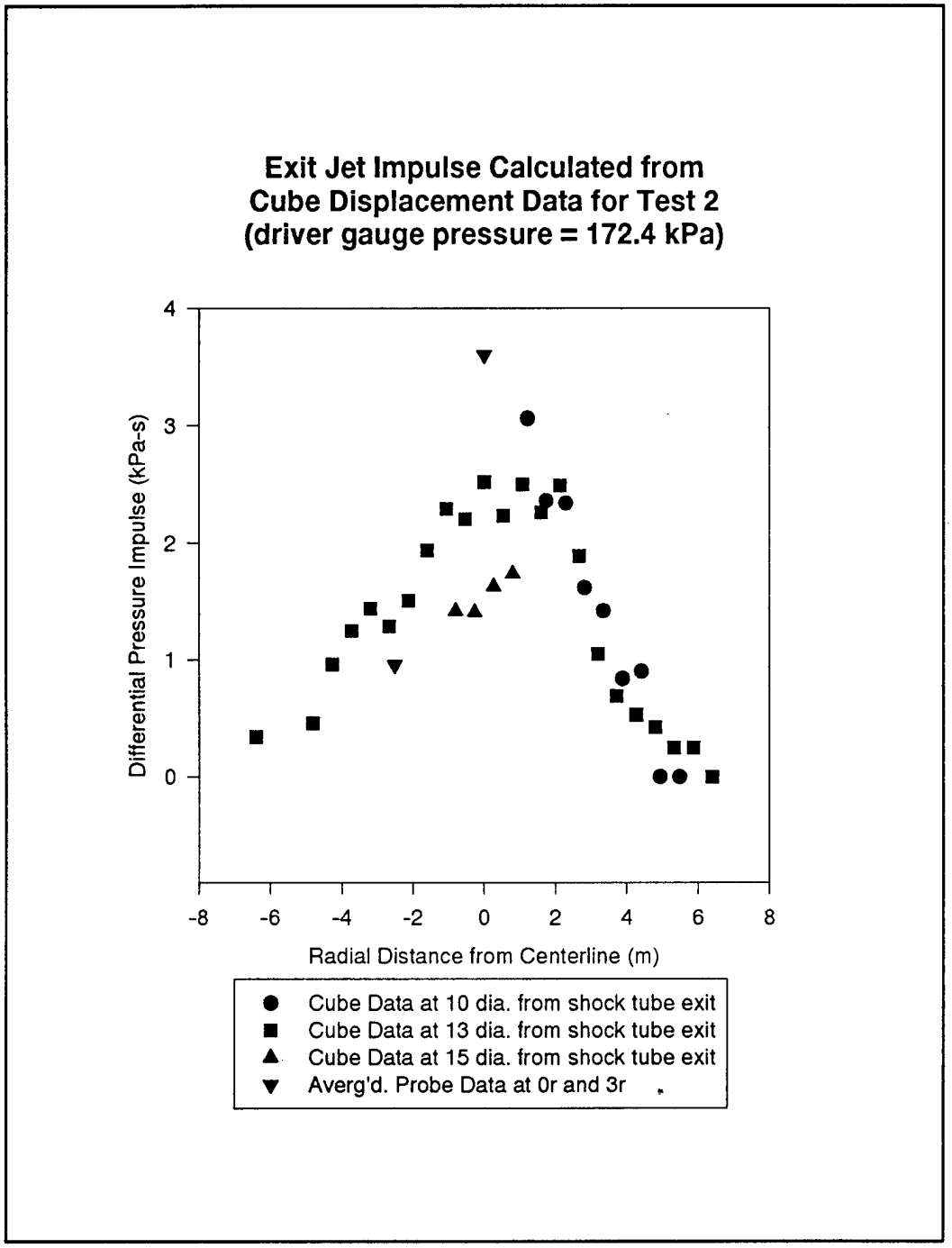

Figure 22. Differential Pressure Impulse Versus Radial Distance for Test 2.

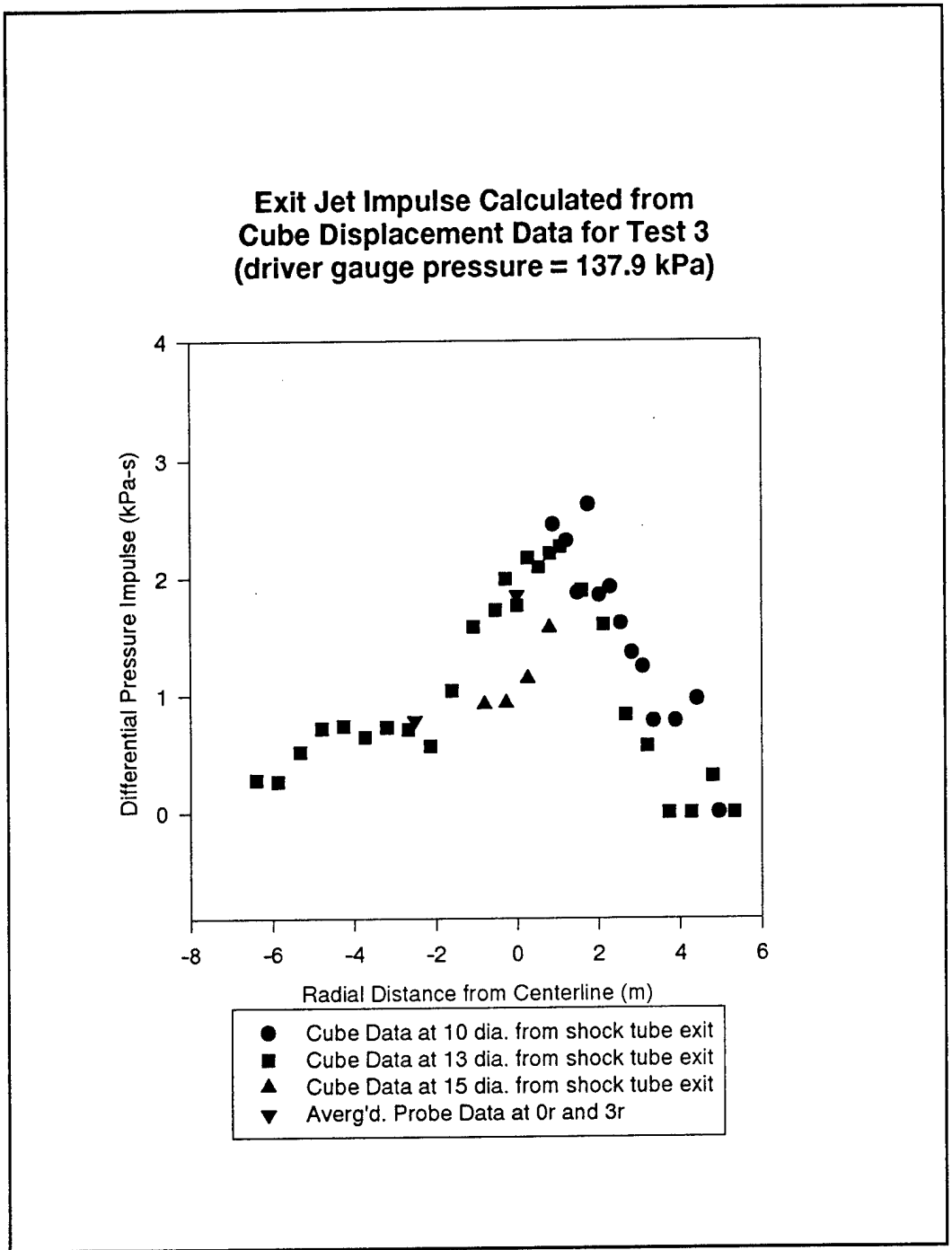

Figure 23. Differential Pressure Impulse Versus Radial Distance for Test 3.

jets in Tests 1 and 2. The average differential pressure impulse in the central region at 10 to 13 diameters was approximately 2.0 kPa-s. The cubes at 15 diameters showed a significant reduction in differential pressure impulse. Figure 24 shows the results for Test 4, the first of the two tests with a jeep included. At this point in the testing, there was reasonable confidence that the dynamic pressure impulse desired for a jeep test had been bracketed by the previous tests as indicated by the differential pressure impulse. The driver gauge pressure was 158.6 kPa (23.0 psi), delivering approximately 2.0 kPa-s at probe rake $0r$ directly in front of the center of mass of the jeep (see Figure 18). Some of the 10-diameter cubes nearest the $+2r$ position indicated a differential pressure impulse around 3.3 kPa-s, possibly because of their being in a part of the jet that had been further accelerated by flowing around the jeep. No cubes were placed along the direct flow path that included the jeep. Finally, Figure 25 shows the results for Test 5, which had a slightly reduced driver gauge pressure of 144.8 kPa (21.0 psi) as compared with Test 4. In Test 5, the jeep was placed so that the center of area, rather than the center of mass, was aligned with the shock tube axis and directly behind the $0r$ probe rake (see Figure 19). The average for probe rake $0r$ indicated a differential pressure impulse of 2.0 kPa-s, the same as that for Test 4, but the cubes at 10 diameters indicated a higher value of about 2.7 kPa-s, but not quite as high as they did for Test 4. Both Tests 4 and 5 showed good symmetry at the $\pm$ $3r$ and greater radial distance ranges for which there were cubes on both sides for comparison. In summarizing all five of these figures, exit jet uniformity seems best between the $\pm$ $2r$ locations, within 10 to 15 diameters from the end of the shock tube.

The locations, measured in the same manner as for the cubes, of the jeeps in Tests 4 and 5 were recorded at the rear (RTC) and front (FTC) tires' centers on the side of the jeep originally facing the exit jet, before and after each test. This allowed the computation of the individual vector displacements referenced at the front and rear wheels. Figure 26 is a photograph showing the jeep's orientation after Test 4. The tire center displacements were 11.66 m (RTC) and 9.66 m (FTC), for a mean displacement of 10.66 m (34.0 ft). Figure 27 is a photograph of the jeep's orientation after Test 5. Here, the tire center displacements were 8.20 m (RTC) and 7.54 m (FTC), for a mean displacement of 7.87 m (25.8 ft). These displacements and video recorded during the tests clearly indicate that Test 4 (driver gauge pressure 158.6 kPa) had a higher dynamic pressure impulse than Test 5 (driver gauge pressure 144.8 kPa). In Test 4, the jeep was rolled while lifted completely off the ground, rotating somewhat about its center of gravity in midair, before coming to rest right side up (total of one 360-degree roll). In Test 5, the jeep simply rolled over one time in a less violent roll, never completely leaving the ground, before coming to rest right side up. These displacements may be compared with past jeep displacement data for near-ideal blast shown in Figure 28 that were recorded during actual nuclear testing and high explosive simulation of nuclear testing and analyzed by Bryant and Allen.[33] As stated previously, the differential pressure impulse recorded in Test 4 ranged from 2.0 kPa-s (pressure data from probe rakes $0r$ and $3r$) to about 3.3 kPa-s (indicated from the cube displacement analysis), with a measured mean jeep displacement of 10.66 m. This is consistent with a displacement range of 3.5 m, $\pm$ 1.5 m for 2.0 kPa-s, to 9.0 m $\pm$ 3 m for 3.3 kPa-s taken from the fitted curve in Figure 28 and estimating the error range from the scattered data points. Similarly, the differential pressure impulse in Test 5 ranged from 2.0 kPa-s (probe rakes $0r$ and $3r$) to about 2.7 kPa-

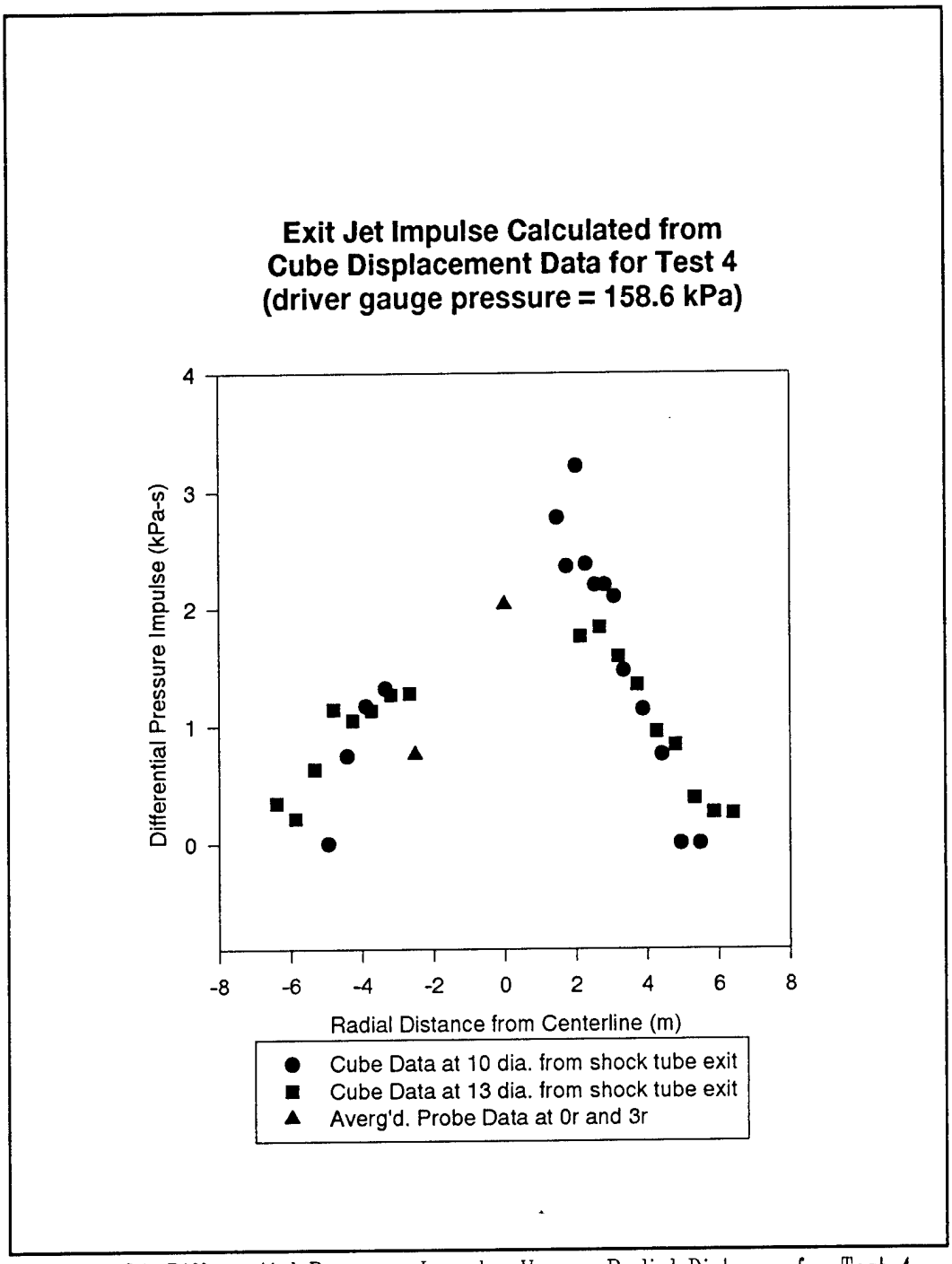

Figure 24. Differential Pressure Impulse Versus Radial Distance for Test 4.

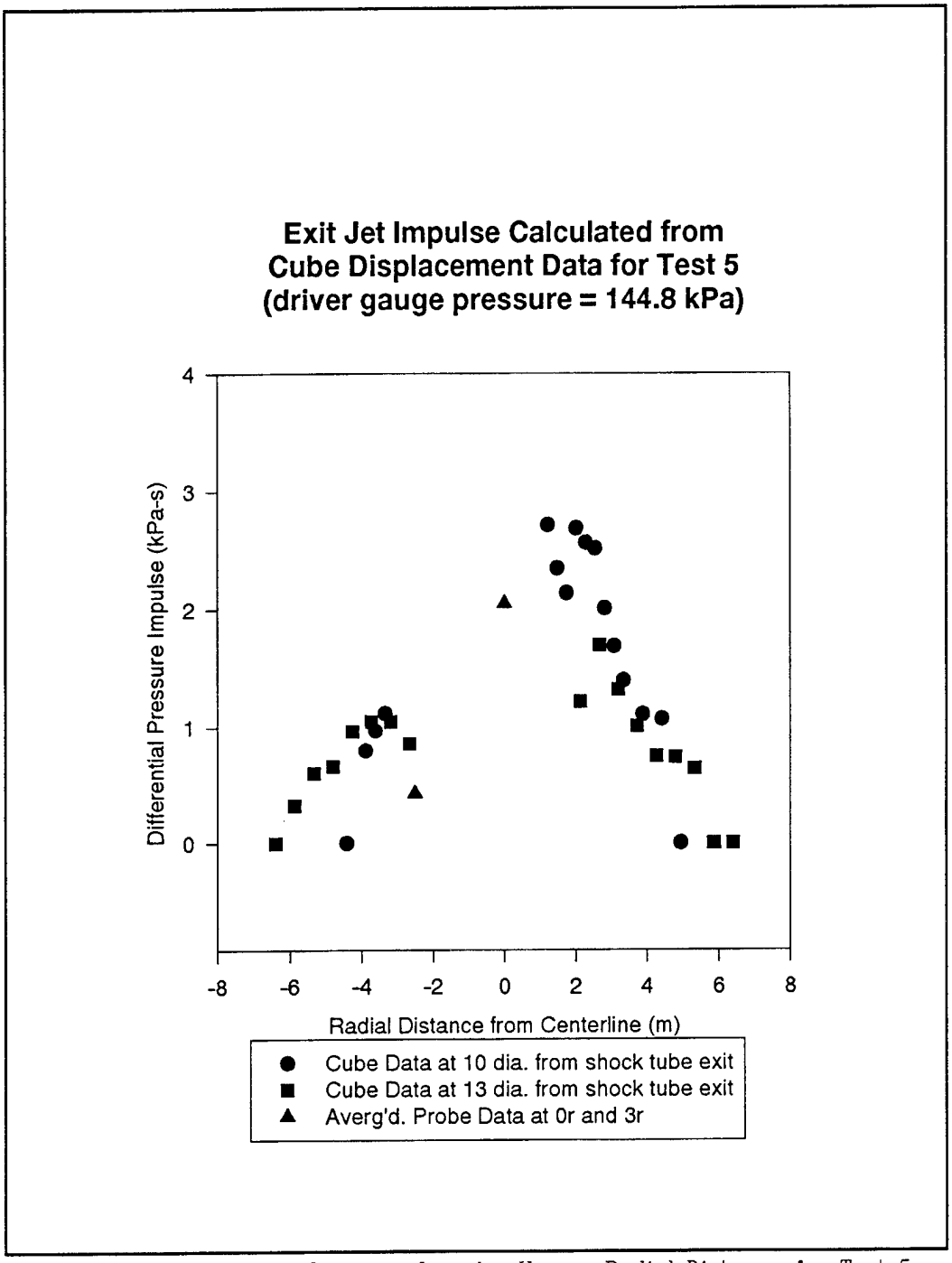

Figure 25. Differential Pressure Impulse Versus Radial Distance for Test 5.

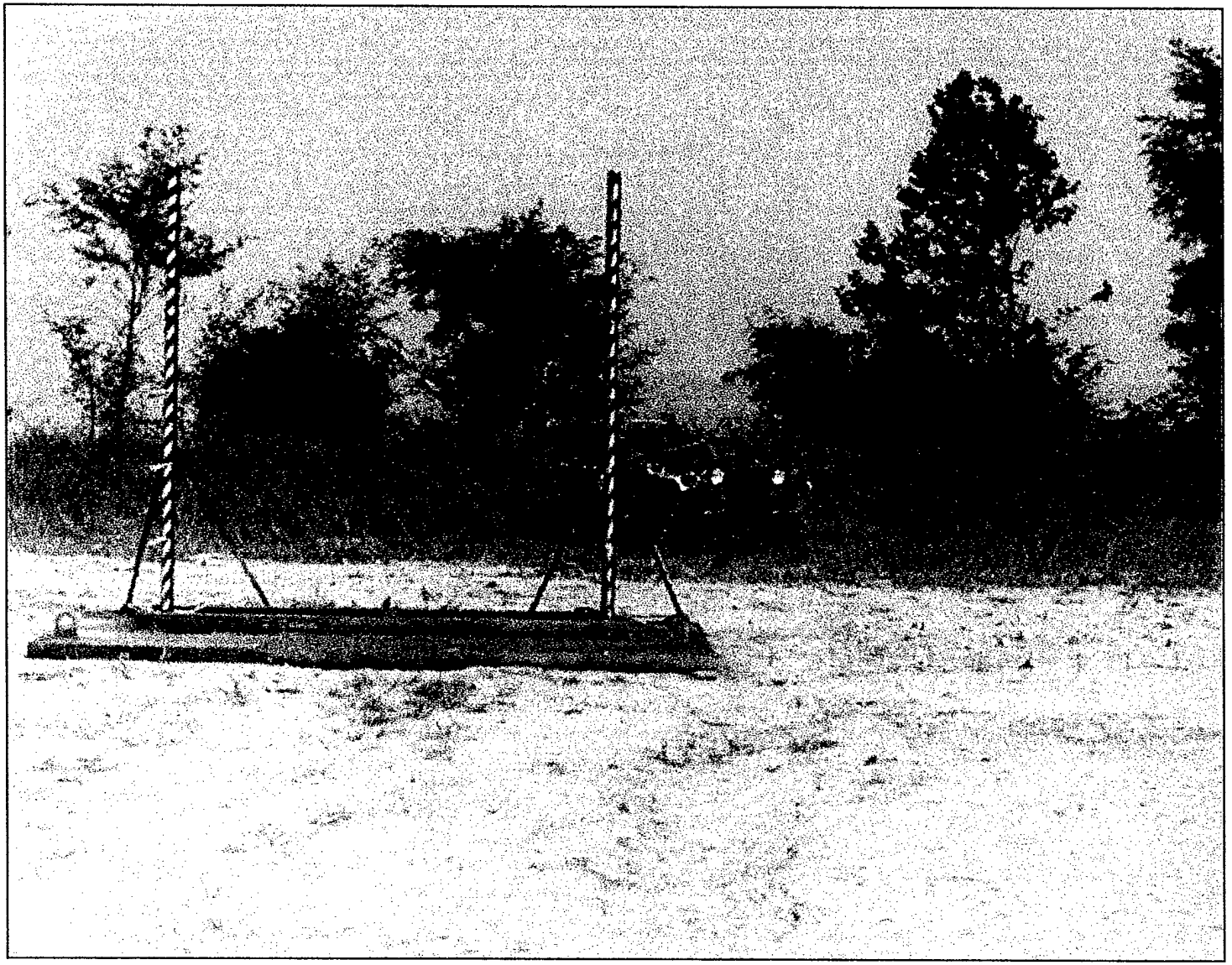

Figure 26. Jeep Final Orientation in Test 4.

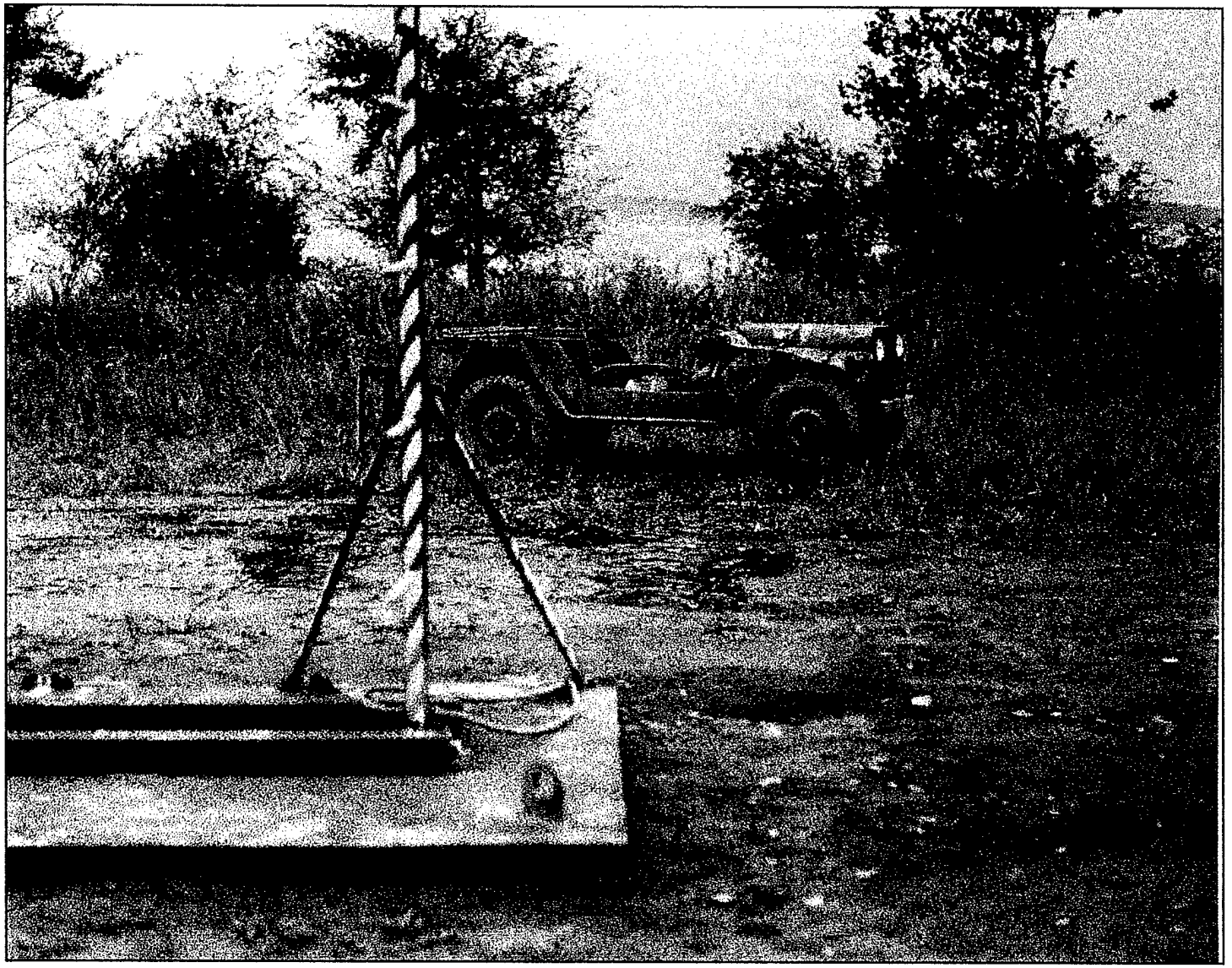

Figure 27. Jeep Final Orientation in Test 5.

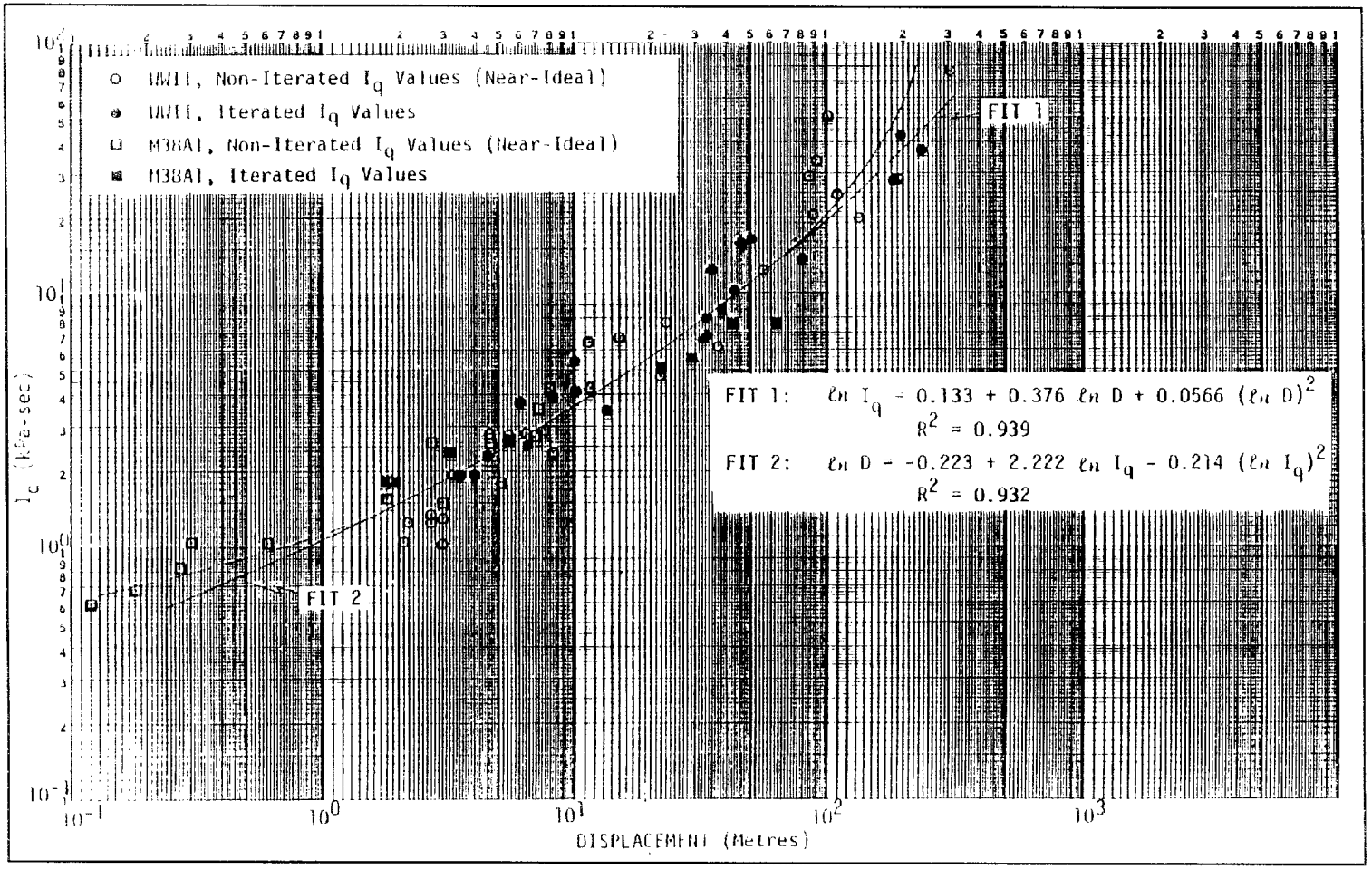

Figure 28. Dynamic Pressure Impulse Versus Displacement – WWII and M38A1, Side-on (unclassified figure from Bryant and Allen, 1981).

s (cube displacement), with a mean jeep displacement of 7.87 m. Using Figure 28 in the same fashion as before, this is consistent with a displacement range of 3.5 m, ± 1.5 m for 2.0 kPa-s, to 5.8 m ± 2.5 m for 2.7 kPa-s. Tests 4 and 5 produced jeep displacements toward the high end of the range, especially if it is assumed that the averaged differential pressure impulse from probe rakes $0r$ and $3r$ is a more reliable indicator than that inferred from the cube displacements. The condition of the surface is a major factor in producing a range of displacements for a given delivery of dynamic pressure impulse. The raised ground plane on which the tests were conducted had just been constructed. It was made from compacted, rolled soil with a large clay content and, for erosion control, had been seeded with grass which had begun a few inches of growth. This produced a level, firm surface that may have allowed more jeep motion than the typical (probably softer and rougher) surfaces of the field tests,[33] and thus tended toward the high end of the range of displacements. The original intention of having a raised ground plane of soil was that, with a minor amount of earth work, any desired surface could be generated for a given experiment. It had already been shown in a computational study by Guidos et al.[19] that the exit jet from the 1.68-m shock tube could be made to simulate a non-ideal blast flow. Similarly, Schraml[23] showed in a computational study that the exit jet from the U.S. LB/TS could also be used to simulate a non-ideal blast flow. This series of demonstration tests with the ARL 1.68 m shock tube provides a strong experimental indication of the viability and validity of the use of shock tube exit jets as one way of simulating the dynamic pressure impulse delivery of non-ideal blast flows on full scale Army tactical vehicles and structures.

6. CONCLUSIONS AND RECOMMENDATIONS

These tests helped to substantiate the capabilities of the exit jet concept in simulating non-ideal nuclear blast events on full scale Army materiel. The full scale spreader successfully delivered a more uniform dynamic pressure impulse than could be delivered from the 1.68-m shock tube without an exit jet spreader but with more improvement in uniformity still needed. Jeep displacement data agreed well with nuclear and high explosive test data. The tests with the jeeps used driver gauge pressures in the range of 152 kPa (22 psi), well below the maximum recent operating pressure of about 552 kPa (80 psi) and the original design operating pressure of 827 kPa (120 psi), so there is considerably more potential in the ARL 1.68-m shock tube, or any similar shock tube, to generate dynamic pressure impulse at levels that pose a credible threat to full scale armored vehicles.[15]

Currently, the ARL shock tubes at Aberdeen Proving Ground are in place but not being actively operated. The 1.68-m shock tube could be put back into operation without much difficulty. Any future testing should at least provide for flush mounting of the probe rake stand with the ground plane, if not resetting of the original concrete reaction mass mounts for the probe rakes. This would minimize local jet flow disturbances in the vicinity of the instrumentation, which would improve simulation capability. Also, it was observed that in the tests with jeeps, the vehicles tended to rotate about their center of gravity only after they were lifted totally off the ground from the dynamic pressure. When the delivered dynamic pressure impulse was at a level such that the jeep only rolled, the evidence of rotation about

an axis normal to the ground was minimal. This was believed reasonable since the ground would tend to resist the torque generated on the jeep by the blast pressure. Therefore, assuming that an ideally uniform dynamic pressure impulse exists across the spread jet front, orienting a vehicle with respect to its center of gravity being aligned with or offset from the jet's centerline should result in minimal changes in displacement.

If the ARL non-ideal blast project is restarted, future work should be conducted in subscale or full scale, or both, to optimize the flow through the exit jet spreader and vane assembly to optimize the resulting dynamic pressure distribution of the spread jet on the target vehicle or equipment. This would entail reconfiguring the vanes themselves within the spreader and testing each configuration. The spreader was designed to allow this with only minor effort and no compromise to its structural integrity. More exhaustive tests would include the recording of data at the $1r$ and $2r$ radial positions within the spread jet at the 10-diameter and 5-diameter ranges. This additional testing would provide for a more thorough pressure and impulse mapping study and aid in the understanding of the exit jets' profiles, flow characteristics, and repeatability in full scale. Additional full scale tests could also be performed on other Army vehicles, including the high mobility multi-purpose wheeled vehicle (HMMWV), the Bradley fighting vehicle (BFV), and possibly the Abrams M1 main battle tank, once the exit jet has been better characterized and optimized. These additional vehicle tests would provide more impulse versus horizontal displacement data and ultimately could be used to improve Army vehicle survivability through optimized tactics and doctrine for use on the future battlefield.

Finally, this technology shows promise to be adapted for use with the LB/TS at White Sands Missile Range. This could be one of a complementing set of ways to use the LB/TS to extend its operating capabilities to include non-ideal blast simulation as well as for the ideal blast simulation it was originally designed to perform.

REFERENCES

1. S. Glasstone and P. Dolan - Editors, "The Effects of Nuclear Weapons," Department of Army Pamphlet No. 50-3, HQ, Department of Army, March 1977.

2. E.J. Bryant and F. Allen, "Dynamic Pressure Impulse for Near Ideal and Non-Ideal Blast Waves," DNA-82-C-0287, Defense Nuclear Agency, Alexandria, VA, November 1983.

3. F.H. Shelton, "Reflections of a Nuclear Weaponeer," ISBN 1-881816-08-8, Shelton Enterprise, Inc., Colorado Springs, CO, 1988.

4. S.R. Hikida, R.L. Bell, and C.E. Needham, "The SHARC Codes: Documentation and Sample Problems," S-Cubed Technical Report SSS-R-89-9878, S-Cubed, Inc., Albuquerque, NM, September 1988.

5. C.E. Needham, R.G. Ekler, and L.W. Kennedy, "Extended Desert Calculation Results with Comparisons to PRISCILLA Experimental Data and a Near-Ideal Calculation," ARL-CR-235, U.S. Army Research Laboratory, APG, MD, July 1995.

6. R.G. Ekler, C.E. Needham, and L.W. Kennedy, "Extended Grassland Calculation Results with Comparisons to PRISCILLA Experimental Data and a Near-Ideal Calculation," ARL-CR-236, U.S. Army Research Laboratory, APG, MD, July 1995.

7. N.H. Ethridge, J.H. Keefer, J.E. Crepeau, R.G. Ekler, L.W. Kennedy, C.E. Needham, S.H. Rogers, "Real Surface (Non-Ideal) Effects on Nuclear Explosion Airblast from PRISCILLA-Type Events, Part I: Comparison and Evaluation of Ideal and Non-Ideal Airblast from PRISCILLA Computations, and Part II: SHARC Hydrocode Calculations of the PRISCILLA Event (Phase I)," ARL-CR-277, U.S. Army Research Laboratory, APG, MD, October 1995.

8. H. Schlichting, "Boundary Layer Theory," Sixth Edition, McGraw-Hill Book Company, NY, 1968.

9. R.J. Pearson, H.L. Wisniewski, P.D. Szabados, A.W. Wilson, "The Effects of Thermal/Blast Synergism on the Nuclear Vulnerability of a Generic Aircraft Structure," ARBRL-TR-02540, U.S. Army Ballistic Research Laboratory, APG, MD, January 1984.

10. R.T. Newell, "Flow Generator Simulation Concept Verification," WA9-239, New Mexico Engineering Research Institute, Albuquerque, NM, September 1987.

11. C.N. Kingery and E.J. Gion, "Jet-Flow from Shock Tubes," BRL-TR-3015, U.S. Army Ballistic Research Laboratory, APG, MD, July 1989.

12. C.N. Kingery and E.J. Gion, "Tunnel-Exit Pressure and Impulse Effects on Free-Field Pressure and Impulse," BRL-TR-3132, U.S. Army Ballistic Research Laboratory, APG, MD, August 1990.

13. E.J. Gion and C.N. Kingery, "Disruption of 0-deg Line Flow Induced by Barricade Fronting a Simulated Explosives Storage Magazine," BRL-TR-3211, U.S. Army Ballistic Research Laboratory, APG, MD, February 1991.

14. C.N. Kingery, "Open End Shock Tube Testing," Presentation, U.S. Army Ballistic Research Laboratory, APG, MD, 1989.

15. Operating log for ARL 1.68-m shock tube, May 1992.

16. N.H. Ethridge, "Proposed Modification of the Jet Flow from the BRL 1.68-m Shock Tube," BRL-CR-664, U.S. Army Ballistic Research Laboratory, APG, MD, May 1991.

17. R.E. Lottero, Communication of proposed design of simple jet spreader, U.S. Army Research Laboratory, APG, MD, July 1994.

18. R.B. Loucks, P.C. Muller, R.L. Thane, T.C. Cline, L.G. Ferguson, and C. Mermagen, "Simulation of Non-Ideal Blast with a Shock Tube Exit Jet," ARL-TR-984, U.S. Army Research Laboratory, APG, MD, February 1996.

19. B.J. Guidos, S.J. Schraml, and D.K. Ota, "Navier-Stokes Computation of Shock Tube Exit Jet for Non-Ideal Blast Simulations," ARL-TR-1105, U.S. Army Research Laboratory, APG, MD, April 1996.

20. J.L. Evans, H.D. Laverentz, C.L. Griffin, A.A. Kramer, S.J. Guislain, "System Integration Study of a Large Blast/Thermal Simulator," Black & Veatch Consulting Engineers, for Defense Nuclear Agency, DNA-TR-86-394, June 87.

21. J.R. Crosnier and J.B.G. Monzac, "Large Diameter High Performance Blast Simulator," Proceedings of the Fifth International Symposium on Military Applications of Blast Simulation, Stockholm, Sweden, 23-26 May 1977.

22. U.S./French Data Exchange Annex MWDDEA-A-80-F-1265, "Nuclear Weapons Effects."

23. S.J. Schraml, "Characterization of Jet Flow from a Decaying Wave Blast Simulator," ARL-TR-1259, U.S. Army Research Laboratory, APG, MD, January 1997.

24. A. Mark, Private communication, U.S. Army Research Laboratory, APG, MD, 1993.

25. R.E. Lottero, "Non-Ideal Blast Phenomenology and Program Plans," as U.S. Associate Technical Project Officer for Nuclear Blast and Thermal, MWDDEA-A-80-F-1265, US and France Technical Exchange Meeting, U.S. Army Research Laboratory, APG, MD 21-22 April 1993.

26. D. Mergnat, D. Tournemine, J.L. Cremoux, "*Simulation au SSGG des Effets des Ondes de Choc et de Souffle Non-Ideales Induites par le Precurseur Thermique lors des Explosions Nucleares*," T-96-04, *Centre d'Etudes de Gramat, France*, January 1996.

27. Logicon, RDA, "Proceedings of the FY97 Non-Ideal Airblast (NIAB) Program Kick-off Meeting," Albuquerque, NM, and Kirtland Air Force Base, NM, April 1997.

28. S.J. Schraml, "Exploratory Analysis of Helium Layer Usage for Dynamic Pressure Enhancement in the Large Blast/Thermal Simulator," ARL-TR-869, U.S. Army Research Laboratory, APG, MD, September 1995.

29. E.A. Avallone and T. Baumeister, Editors, "Mark's Standard Handbook for Mechanical Engineers," Ninth Edition, McGraw-Hill Book Company, New York, NY, 1986.

30. ALGOR Accupak Reference Manual, Part Number 6700.401, ALGOR Inc., 150 Beta Drive, Pittsburgh, PA, October 1994.

31. N.H. Ethridge, and J.H. Keefer, Private communication: design, layout, and analysis for cube displacement study, as retired scientists from the former U.S. Army Ballistic Research Laboratory, APG, MD, September/October 1997.

32. A.K. Faizullabhoy and P.J. Westwick, "Operational Guide to High Explosive Tests from DICE THROW (October 1976) through DISTANT IMAGE (May 1991)," DASIAC-SR-92-010, Defense Nuclear Agency, Alexandria, VA, June 93.

33. E.J. Bryant and F.J. Allen, "Dynamic Pressure Impulse for Near-Ideal and Non-Ideal Blast Waves - Height of Burst Charts, (U)," DNA-5826F, Defense Nuclear Agency, Alexandria, VA, May 1981 (CONFIDENTIAL).

INTENTIONALLY LEFT BLANK

NO. OF COPIES	ORGANIZATION
2	ADMINISTRATOR DEFENSE TECHNICAL INFO CENTER ATTN DTIC DDA 8725 JOHN J KINGMAN RD STE 0944 FT BELVOIR VA 22060-6218
1	DIRECTOR US ARMY RESEARCH LABORATORY ATTN AMSRL OP SD TA/ RECORDS MANAGEMENT 2800 POWDER MILL RD ADELPHI MD 20783-1197
1	DIRECTOR US ARMY RESEARCH LABORATORY ATTN AMSRL OP SD TL/ TECHNICAL LIBRARY 2800 POWDER MILL RD ADELPHI MD 207830-1197
1	DIRECTOR US ARMY RESEARCH LABORATORY ATTN AMSRL OP SD TP/ TECH PUBLISHING BRANCH 2800 POWDER MILL RD ADELPHI MD 20783-1197
2	DIRECTOR FEDERAL EMERGENCY MGMT AGENCY ATTN PUBLIC RELATIONS OFFICE TECHNICAL LIBRARY WASHINGTON DC 20472
1	CHAIRMAN DOD EXPLOSIVES SAFETY BOARD ROOM 856 C HOFFMAN BLDG 1 2461 EISENHOWER AVENUE ALEXANDRIA VA 22331-0600
1	DIRECTOR OF DEFENSE RESEARCH AND ENGINEERING ATTN DD/TWP WASHINGTON DC 20301
1	ASST SECRETARY OF DEFENSE (ATOMIC ENERGY ATTN DOCUMENT CONTROL WASHINGTON DC 20301
1	CHAIRMAN JOINT CHIEFS OF STAFF ATTN J 5 R&D DIVISION WASHINGTON DC 20301

NO. OF COPIES	ORGANIZATION
6	DIRECTOR DEFENSE SPECIAL WEAPONS AGENCY ATTN CSTI TECHNICAL LIBRARY ESA W SUMMA J O'SHAUGHNESSY K PETERSEN WEP T KENNEDY M FRANKEL WASHINGTON DC 20305
2	DA DCSOPS ATTN TECHNICAL LIBRARY DIR OF CHEM & NUC OPS WASHINGTON DC 20310
4	COMMANDER FIELD COMMAND DSWA ATTN FCTTS E MARTINEZ FCTOSL F MOYNIHAN FCTIH H ROSS FCTIH W BRENNAN KIRTLAND AFB NM 87115
10	CENTRAL INTELLIGENCE AGENCY DIR/DB/STANDARD ATTN GE 47 HQ WASHINGTON DC 20505
1	DIRECTOR ADVANCED RSCH PROJECTS AGENCY ATTN TECHNICAL LIBRARY 3701 NORTH FAIRFAX DRIVE ARLINGTON VA 22203-1714
2	COMMANDER US ARMY CECOM ATTN AMSEL RD AMSEL RO TPPO P FORT MONMOUTH NJ 07703-5301
1	COMMANDER US ARMY CECOM R&D TECHNICAL LIBRARY ATTN ASQNC ELC IS L R MYER CTR FORT MONMOUTH NJ 07703-5000
1	MIT ATTN TECHNICAL LIBRARY CAMBRIDGE MA 02139
1	COMMANDER US ARMY FSTC ATTN RESEARCH & DATA BRANCH 220 7TH STREET NE CHARLOTTESVILLE VA 22901-5396

NO. OF COPIES	ORGANIZATION
1	COMMANDER US ARMY ARDEC ATTN SMCAR FSM W/BARBER BLDG94 PICATINNY ARSENAL NJ 07806-5000
1	DIRECTOR US ARMY MISSILE & SPACE INTELLIGENCE CENTER ATTN AIAMS YDL REDSTONE ARSENAL AL 35898-5500
1	COMMANDING OFFICER (CODE L51) NAVAL CIVIL ENGINEERING LAB ATTN J TANCRETO PORT HUENEME CA 93043-5003
2	COMMANDER US ARMY STRATEGIC DEFENSE CMD ATTN CSSD H MPL TECH LIB CSSD H XM DR DAVIES PO BOX 1500 HUNTSVILLE AL 35807
2	COMMANDER US ARMY CORPS OF ENGINEERS WATERWAYS EXPERIMENT STA ATTN CEWES SS R J WATT CEWES TL TECH LIBRARY PO BOX 631 VICKSBURG MS 39180-0631
1	COMMANDER US ARMY ENGINEER DIVISION ATTN HNDED FD PO BOX 1500 HUNTSVILLE AL 35807
3	COMMANDER US ARMY NUCLEAR & CHEM AGENCY 7150 HELLER LOOP SUITE 101 SPRINGFIELD VA 22150-3198
1	COMMANDER US ARMY CORPS OF ENGINEERS FT WORTH DISTRICT ATTN CESWF PM J PO BOX 17300 FORT WORTH TEXAS 76102-0300
1	DIRECTOR TRAC FLVN ATTN ATRC FORT LEAVENWORTH KS 66027-5200

NO. OF COPIES	ORGANIZATION
1	COMMANDER US ARMY RESEARCH OFFICE ATTN SLCRO D PO BOX 12211 RESEARCH TRIANGLE PARK NC 27709-2211
1	DIRECTOR HQ TRAC RPD ATTN ATRC RPR RADDA FORT MONROE VA 23651-5143
2	OFFICE OF NAVAL RESEARCH ATTN DR A FAULSTICK CODE 23 800 N QUINCY STREET ARLINGTON VA 22217
1	DIRECTOR TRAC WSMR ATTN ATRC WC KIRBY WSMR NM 88002-5502
2	COMMANDER US ARMY WSMR ATTN STEWS NED (DR MEASON) STEWS DATTS O (RL PENNY) WSMR NM 88002-5158
2	CHIEF OF NAVAL OPERATIONS DEPARTMENT OF THE NAVY ATTN OP 03EG OP 985F WASHINGTON DC 20350
1	COMMANDER DAVID TAYLOR RESEARCH CENTER ATTN CODE 522 TECH INFO CTR BETHESDA MD 20084-5000
1	OFFICER IN CHARGE (CODE L31) CIVIL ENGINEERING LABORATORY NAVAL CONST BATTALION CENTER ATTN TECHNICAL LIBRARY PORT HUENEME CA 93041
1	COMMANDER (CODE 533) NAVAL WEAPONS CENTER ATTN TECHNICAL LIBRARY CHINA LAKE CA 93555-6001
1	COMMANDER DAHLGREN DIVISION NAVAL SURFACE WARFARE CENTER ATTN CODE E23 LIBRARY DAHLGREN VA 22448-5000

NO. OF COPIES	ORGANIZATION
1	COMMANDER NAVAL RESEARCH LABORATORY ATTN CODE 2027 TECH LIBRARY WASHINGTON DC 20375
1	OFFICER IN CHARGE WHITE OAK WARFARE CENTER DETACHMENT ATTN CODE E232 TECH LIBRARY 10901 NEW HAMPSHIRE AVENUE SILVER SPRING MD 20903-5000
1	AL/LSCF ATTN J LEVINE EDWARDS AFB CA 93523-5000
1	COMMANDER NAVAL WEAPONS EVALUATION FAC ATTN DOCUMENT CONTROL KIRTLAND AFB NM 87117
1	RADC (EMTLD/DOCUMENT LIB) GRIFFISS AFB NY 13441
1	AEDC ATTN R MCAMIS MAIL STOP 980 ARNOLD AFB TN 37389
1	OLAC PL/TSTL ATTN D SHIPLETT EDWARDS AFB CA 93523 5000
1	AFIT/ENY ATTN LTC HASEN PHD WRIGHT PATTERSON AFB OH 45433-6583
2	AIR FORCE ARMAMENT LAB ATTN AFATL/DOIL AFATL/DLYV EGLIN AFB FL 32542-5000
1	DIRECTOR LAWRENCE LIVERMORE NATL LAB ATTN TECH INFO DEPT L 3 PO BOX 808 LIVERMORE CA 94550
1	NAIC/DXLA ATTN TECHNICAL LIBRARY 4180 WATSON WAY WRIGHT PATTERSON AFB OH 45433-5648

NO. OF COPIES	ORGANIZATION
1	DIRECTOR NATL AERONAUTICS & SPACE ADMIN ATTN SCIENTIFIC & TECH INFO FAC PO BOX 8757 BWI AIRPORT BALTIMORE MD 21240
3	KAMAN SCIENCES CORPORATION ATTN LIBRARY PA ELLIS FH SHELTON PO BOX 7463 COLORADO SPRINGS CO 80933-7463
4	DIRECTOR IDAHO NATIONAL ENGINEERING LAB EG&G IDAHO INC ATTN R GUENZLER MS 3505 R HOLMAN MS 3510 R A BERRY W C REED PO BOX 1625 IDAHO FALLS ID 83415
4	DIRECTOR SANDIA NATIONAL LABORATORIES ATTN DOC CONTROL 3141 D GARDNER DIV 1421 J MCGLAUN DIV 1541 PO BOX 58O0 ALBUQUERQUE NM 87185-5800
2	LOS ALAMOS NATL LABORATORY MAIL STATION 5000 REPORT COLLECTION CID 14 MS P364 PO BOX 1663 LOS ALAMOS NM 87545
1	REPORT COLLECTION CIC 14 MS P364 LOS ALAMOS NATL LABORATORY LOS ALAMOS NM 87545
1	REPORT COLLECTION RESEARCH LIBRARY MS P362 PO BOX 7113 LOS ALAMOS NM 87544-7113
1	DIRECTOR SANDIA NATIONAL LABORATORIES LIVERMORE LABORATORY ATTN DOC CONTROL FOR TECH LIB PO BOX 969 LIVERMORE CA 94550

NO. OF COPIES	ORGANIZATION
1	DIRECTOR NASA LANGLEY RESEARCH CENTER ATTN TECHNICAL LIBRARY HAMPTON VA 23665
2	APPLIED RESEARCH ASSOCIATES INC ATTN J KEEFER NH ETHRIDGE PO BOX 548 ABERDEEN MD 21001
4	APPLIED RESEARCH ASSOCIATES INC ATTN C NEEDHAM J CREPEAU S HIKIDA R NEWELL 4300 SAN MATEO BLVD ALBUQUERQUE NM 87110
1	ADA TECHNOLOGIES INC ATTN JAMES R BUTZ HONEYWELL CENTER SUITE 110 304 INVERNESS WAY SOUTH ENGLEWOOD CO 80112
1	CARPENTER RESEARCH CORP ATTN H JERRY CARPENTER 27520 HAWTHORNE BLVD SUITE 263 PO BOX 2490 ROLLING HILLS ESTATES CA 90274
1	AEROSPACE CORPORATION ATTN TECH INFO SERVICES PO BOX 92957 LOS ANGELES CA 90009
1	THE BOEING COMPANY ATTN AEROSPACE LIBRARY PO BOX 3707 SEATTLE WA 98124
2	FMC CORPORATION ADVANCED SYSTEMS CENTER ATTN J DROTLEFF C KREBS MDP 95 BOX 58123 2890 DE LA CRUZ BLVD SANTA CLARA CA 95052
1	SVERDRUP TECHNOLOGY INC SVERDRUP CORPORATION AEDC ATTN BD HEIKKINEN MS 900 ARNOLD AFB TN 37389-9998

NO. OF COPIES	ORGANIZATION
1	DYNAMICS TECHNOLOGY INC ATTN D T HOVE G P MASON 21311 HAWTHORNE BLVD SUITE 300 TORRANCE CA 90503
1	EATON CORPORATION DEFENSE VALVE & ACTUATOR DIV ATTN J WADA 2338 ALASKA AVE EL SEGUNDO CA 90245-4896
2	MCDONNELL DOUGLAS ASTRO- NAUTICS CORP ATTN R W HALPRIN K A HEINLY 5301 BOLSA AVENUE HUNTINGTON BEACH CA 92647
4	KAMAN AVIDYNE ATTN R RUETENIK S CRISCIONE R MILLIGAN T STAGLIANO 83 SECOND AVENUE NORTHWEST INDUSTRIAL PARK BURLINGTON MA 01830
1	MDA ENGINEERING INC ATTN DR DALE ANDERSON 2406 LAKEVIEW CIR ARLINGTON TX 76013-3326
2	POINTWISE INC ATTN J CHAWNER J STEINBRENNER PO BOX 210698 BEDFORD TX 76095-7698
2	PHYSICS INTERNATIONAL CORP PO BOX 5010 SAN LEANDRO CA 94577-0599
2	KAMAN SCIENCES CORPORATION ATTN DASIAC (2CYS) PO DRAWER 1479 816 STATE STREET SANTA BARBARA CA 93102-1479
1	LOGICON RDA ATTN GP GANONG PO BOX 9377 ALBUQUERQUE NM 87119

NO. OF COPIES	ORGANIZATION
1	LOGICON RDA ATTN B LEE 6053 W CENTURY BLVD LOS ANGELES CA 90045
1	SCIENCE CENTER ROCKWELL INTERNATIONAL CORP ATTN S RAMAKRISHNAN D OTA 1049 CAMINO DOS RIOS PO BOX 2085 THOUSAND OAKS CA 91358
1	METACOMP TECHNOLOGIES INC ATTN S CHAKRAVARTHY 650 WESTLAKE BLVD SUITE 203 WESTLAKE VILLAGE CA 91362
1	ORLANDO TECHNOLOGY INC ATTN D MATUSKA 60 SECOND STREET BLDG 5 SHALIMAR FL 32579
4	S CUBED A DIVISION OF MAXWELL LABS INC ATTN TECHNICAL LIBRARY R DUFF K PYATT J BARTHEL PO BOX 1620 LA JOLLA CA 92037-1620
1	SAICORPORATION ATTN J GUEST 2301 YALE BLVD SE SUITE E ALBUQUERQUE NM 87106
1	SUNBURST RECOVERY INC ATTN DR C YOUNG PO BOX 2129 STEAMBOAT SPRINGS CO 80477
1	SVERDRUP TECHNOLOGY INC ATTN RF STARR PO BOX 884 TULLAHOMA TN 37388
1	S CUBED A DIVISION OF MAXWELL LABS INC ATTN JAMES SEVIER 2501 YALE BLVD SE ALBUQUERQUE NM 87106

NO. OF COPIES	ORGANIZATION
3	SRI INTERNATIONAL ATTN DR GR ABRAHAMSON DR J GRAN DR B HOLMES 333 RAVENWOOD AVENUE MENLO PARK CA 94025
1	TRW BALLISTIC MISSILE DIVISION ATTN H KORMAN MAIL STATION 526/614 PO BOX 1310 SAN BERNADINO CA 92402
1	BATTELLE ATTN TACTEC LIB JN KHIGGINS 505 KING AVENUE COLUMBUS OH 43201-2693
1	THERMAL SCIENCE INC ATTN R FELDMAN 2200 CASSENS DRIVE ST LOUIS MO 63026
2	DENVER RESEARCH INSTITUTE ATTN J WISOTSKI TECHNICAL LIBRARY PO BOX 10758 DENVER CO 80210
1	STATE UNIVERSITY OF NEW YORK MECH & AEROSPACE ENGINEERING ATTN DR PEYMAN GIVI BUFFALO NY 14260
2	UNIVERSITY OF MARYLAND INST FOR ADV COMPUTER STUDIES ATTN L DAVIS G SOBIESKI COLLEGE PARK MD 20742
1	CALIFORNIA INST OF TECHNOLOGY ATTN T J AHRENS 1201 E CALIFORNIA BLVD PASADENA CA 91109
1	UNIVERSITY OF MINNESOTA ARMY HIGH PERF COMP RES CTR ATTN DR TAYFUN E TEZDUYAR 1100 WASHINGTON AVE SOUTH MINNEAPOLIS MN 55415

NO. OF COPIES	ORGANIZATION
3	SOUTHWEST RESEARCH INSTITUTE ATTN DR C ANDERSON S MULLIN A B WENZEL PO DRAWER 28255 SAN ANTONIO TX 78228-0255
2	COMMANDER US ARMY NRDEC ATTN SSCNC YSD (J ROACH) SSCNC WST (A MURPHY) KANSAS STREET NATICK MA 10760-5018
1	CECOM SP & TERRESTRIAL COM DIV ATTN AMSEL RD ST MC M H SOICHER FT MONMOUTH NJ 07703-5203
1	PRIN DPTY FOR TECH GY HDQ US ARMY MATL CMND ATTN AMCDCG T M FISETTE 5001 EISENHOWER AVE ALEXANDRIA VA 22333-0001
1	PRIN DPTY FOR ACQTN HDQ US ARMY MATL CMND ATTN AMCDCG A D ADAMS 5001 EISENHOWER AVE ALEXANDRIA VA 22333-0001
1	DPTY CG FOR RDE HDQ US ARMY MATL CMND ATTN AMCRD BG BEAUCHAMP 5001 EISENHOWER AVE ALEXANDRIA VA 22333-0001
1	DPTY ASST SCY FOR RSRCH & TECH SARD-TT F MILTON RM 3E479 THE PENTAGON WASHINGTON DC 20310-0103
1	DPTY ASST SCY FOR RSRCH & TECH SARD-TT D CHAIT THE PENTAGON WASHINGTON DC 20310-0103
1	DPTY ASST SCY FOR RSRCH & TECH SARD-TT K KOMINOS THE PENTAGON WASHINGTON DC 20310-0103
1	DPTY ASST SCY FOR RSRCH & TECH SARD-TT B REISMAN THE PENTAGON WASHINGTON DC 20310-0103
1	DPTY ASST SCY FOR RSRCH & TECH SARD-TT T KILLION THE PENTAGON WASHINGTON DC 20310-0103
1	ODCSOPS D SCHMIDT WASHINGTON DC 20310-1001
1	OSD OUSD(A&T)/ODDDR&E(R) J LUPO THE PENTAGON WASHINGTON DC 20301-7100
1	ARL ELECTROMAG GROUP CAMPUS MAIL CODE F0250 A TUCKER UNIVERSITY OF TEXAS AUSTIN TX 78712
1	DUSD SPACE 1E765 J G MCNEFF 3900 DEFENSE PENTAGON WASHINGTON DC 20301-3900
1	USAASA MOAS-AI W PARRON 9325 GUNSTON RD STE N319 FT BELVOIR VA 22060-5582
1	CECOM PM GPS COL S YOUNG FT MONMOUTH NJ 07703
1	GPS JOINT PROG OFC DIR COL J CLAY 2435 VELA WAY STE 1613 LOS ANGELES AFB CA 90245-5500
1	ELECTRONIC SYSTEMS DIV DIR CECOM RDEC J NIEMELA FT MONMOUTH NJ 07703
3	DARPA L STOTTS J PENNELLA B KASPAR 3701 N FAIRFAX DR ARLINGTON VA 22203-1714

NO. OF COPIES	ORGANIZATION
1	SPECIAL ASST TO THE WING CDR 50SW/CCX CAPT P H BERNSTEIN 300 O'MALLEY AVE STE 20 FALCON AFB CO 80912-3020
1	USAF SMC/CED DMA/JPO M ISON 2435 VELA WAY STE 1613 LOS ANGELES AFB CA 90245-5500
1	US DEPT OF ENERGY ATTN TECH LIB KK 22 K SISSON WASHINGTON DC 20585
1	THE JOHNS HOPKINS UNIV ATTN TECH LIB APPLIED PHYSICS LAB JOHNS HOPKINS ROAD LAUREL MD 20707
8	UNIV OF MARYLAND ATTN ENGR & TECH LIB DR J WALLACEDR P BERNARD DR J DUNCAN DR L ONG DR K KEIGER DR R CALABRESE DR E MAGRAB DR R DICK RM 2168 ENGRG CLASSROOM BLDG COLLEGE PARK MD 20742-5121
1	US NAVAL ACADEMY ATTN R SMITH 363 RICKOVER HALL 590 HOLLOWAY ROAD ANNAPOLIS MD 21402-5002
3	US NAVAL ACADEMY ATTN TECH LIBRARY DR P MCCOY LT D FULLER 572 HOLLOWAY ROAD ANNAPOLIS MD 21402-5002
1	COMMANDING OFFICER NMCB23 6205 STUART ROAD SUITE 101 FT BELVOIR VA 22060-5275
1	OLIN ORDNANCE ATTN TECH LIB J KIBIGER PRODUCT MATERIAL CONTROL 10101 9TH ST N ST PETERSBURG FL 33716

NO. OF COPIES	ORGANIZATION
1	OIR CSB CRB ATTN A M JONES RM 1413 OHB WASHINGTON DC 20505
	ABERDEEN PROVING GROUND
2	DIR ARL ATTN AMSRL OP AP L (TECH LIB) BLDG 305 APG
1	COMMANDER US ARMY TECOM ATTN AMSTE TE F (L TELETSKI) RYAN BLDG APG
1	COMMANDER US ARMY THAMA ATTN AMSTH TE APG -EA
1	COMMANDER US ARMY TEST CENTER ATTN STEC LI APG
53	DIRECTOR US ARMY RESEARCH LABORATORY ATTN AMSRL CS TT J POLK AMSRL HR S L G FERGUSON AMSRL IS CS A MARK AMSRL IS EE R CIANO K DEACON D GARVEY P GILLESPIE R LOUCKS (5 CYS) J MARTIN R MEYERS S NILES R PINNICK A WETMORE AMSRL IS ES COL PRICE AMSRL SC SS R PEARSON AMSRL SE SA M FONG J GERBER T PHAM K TRAN AMSRL WM PB B GUIDOS AMSRL WM T W MORRISON AMSRL WM TA A MIHALCIN AMSRL WM TB K BENJAMIN V BOYLE T CLINE T DORSEY R FREY W HILLSTROM W LAWRENCE R LOTTERO (5 CYS) E MCDOUGAL J STARKENBERG J SULLIVAN W SUNDERLAND J WATSON AMSRL WM TC W DEROSSET S SCHRAML AMSRL WM W C MURPHY AMSRL WM WB J CONDON (5 CYS) W D'AMICO P MULLER AMSRL WM WF C MERMAGEN

INTENTIONALLY LEFT BLANK

REPORT DOCUMENTATION PAGE

Form Approved
OMB No. 0704-0188

1. AGENCY USE ONLY *(Leave blank)*	2. REPORT DATE	3. REPORT TYPE AND DATES COVERED
	June 1997	Final

4. TITLE AND SUBTITLE
Construction and Testing of the ARL 1.68-m Diameter Shock Tube Exit Jet Spreader for Non-Ideal Blast Simulation

5. FUNDING NUMBERS
PR: 1L162618AH80
NDE203

6. AUTHOR(S)
Condon, J.A.; Lottero, R.E.; Loucks, R.B.

7. PERFORMING ORGANIZATION NAME(S) AND ADDRESS(ES)
U.S. Army Research Laboratory
Weapons & Materials Research Directorate
Aberdeen Proving Ground, MD 21010-5066

8. PERFORMING ORGANIZATION REPORT NUMBER

9. SPONSORING/MONITORING AGENCY NAME(S) AND ADDRESS(ES)
U.S. Army Research Laboratory
Weapons & Materials Research Directorate
Aberdeen Proving Ground, MD 21010-5066

10. SPONSORING/MONITORING AGENCY REPORT NUMBER
ARL-TR-1336

11. SUPPLEMENTARY NOTES

12a. DISTRIBUTION/AVAILABILITY STATEMENT
Approved for public release; distribution is unlimited.

12b. DISTRIBUTION CODE

13. ABSTRACT *(Maximum 200 words)*

The U.S. Army Research Laboratory (ARL) has demonstrated the feasibility of using the modified exit jet of a simple shock tube to simulate high dynamic pressure air blast flows such as those that occur in non-ideal nuclear blast events. These flows can be used to generate simulated non-ideal blast loads on Army equipment with the intent of evaluating and improving its survivability. This work has included the use of small, intermediate, and large scale shock tubes to which exit jet spreader devices were incorporated. These spreaders were mounted at the ends of the shock tubes but were not directly connected to them. Their purpose was to spread the exit jets and their associated dynamic pressure impulses more uniformly over a greater area, thus providing a more accurate simulation capability for testing larger targets.

This report documents some of the latest efforts by ARL in evaluating the use of modified shock tube exit jets for simulating non-ideal blast flow. Previous studies at ARL included the mapping of unspread exit jets at three different shock tube scaled sizes and the evaluation of exit jet spreaders at the two smaller shock tube sizes to evaluate the effectiveness of the various spreaders and determine the degree of uniformity of the spreading. In the latest effort, a full scale exit jet spreader has been constructed for use with the ARL 1.68-m diameter shock tube, the largest of the three shock tubes. Displacement experiments with World War II Army jeeps have been conducted to compare vehicle response to the dynamic pressure impulse loading generated by the spread jet of the shock tube with that from past actual and simulated nuclear tests in which jeep displacement data were obtained.

14. SUBJECT TERMS		15. NUMBER OF PAGES
air blast non-ideal blast	shock tube	70
		16. PRICE CODE

17. SECURITY CLASSIFICATION OF REPORT	18. SECURITY CLASSIFICATION OF THIS PAGE	19. SECURITY CLASSIFICATION OF ABSTRACT	20. LIMITATION OF ABSTRACT
Unclassified	Unclassified	Unclassified	